Schweizerische Eidgenossenschaft
Confédération suisse
Confederazione Svizzera
Confederaziun svizra

Eidgenössisches Departement des Innern EDI
Bundesamt für Meteorologie und Klimatologie MeteoSchweiz

Arbeitsbericht MeteoSchweiz Nr. 216

Extreme wind storms over Europe: Statistical Analyses of ERA-40

P.M. Della-Marta, H. Mathis, C. Frei, M.A. Liniger, C. Appenzeller

Arbeitsbericht MeteoSchweiz Nr. 216

Extreme wind storms over Europe: Statistical Analyses of ERA-40

P.M. Della-Marta, H. Mathis, C. Frei, M.A. Liniger, C. Appenzeller

Bitte zitieren Sie diesen Arbeitsbericht folgendermassen
Della-Marta, P.M., Mathis, H., Frei, C., Liniger, M.A., Appenzeller, C.: 2007, Extreme wind storms over Europe: Statistical Analyses of ERA-40, *Arbeitsberichte der MeteoSchweiz*, 216, 79pp.

Herausgeber
Bundesamt für Meteorologie und Klimatologie, MeteoSchweiz, © 2007

MeteoSchweiz
Krähbühlstrasse 58
CH-8044 Zürich
T +41 44 256 91 11
www.meteoschweiz.ch

Weitere Standorte
CH-8058 Zürich-Flughafen
CH-6605 Locarno Monti
CH-1211 Genève 2
CH-1530 Payerne

Abstract

Accurate assessment of the magnitude and frequency of extreme wind speed is of fundamental importance for many safety, engineering and financial applications. We utilise the spatial and temporal consistency of the European Center for Medium Range Forecasts ERA-40 reanalysis data to determine the frequency of extreme winds over the eastern North Atlantic and Europe. The analysis of extreme winds follows two different view points: In a spatially distributed view, wind storm statistics are determined individually at each grid point over the domain, resulting in recurrence estimates of storms for each reanalysis grid point. In an integral, more generalized view, the storm statistics are determined from extreme wind indices that summarize storm magnitude and spatial extent. We investigated the quality of ERA-40 wind gust data, a parameterised forecast field, and found the wind gust values over areas of complex orography to be unrealistic. This led to the need to mask these areas from further analysis. We also used the 850hPa geostrophic wind speed which was found not to suffer from the same problems as wind gust.

We applied classical peak over threshold (POT) extreme value analysis techniques to the extreme wind data. The POT series were first declustered using an automatic declustering technique and then modelled using a Generalised Pareto Distribution (GPD) which was fitted using maximum likelihood estimation (MLE). The uncertainty in the return level and return period of extreme winds was calculated using a number of different methods including the standard delta method, bootstrap resampling and likelihood profile methods.

Extreme wind index (EWI) based return period estimates of prominent European storms range from approximately 0.3 to 100 years whereas grid point based return period estimates range from 0.3 to 1000+ years. The return period estimates derived from EWIs show a high dependence on the domain over which the indices are calculated, with generally higher returns periods for a given storm when considering land grid points compared to the calculations based on the whole domain. EWI based return period estimates show greater dependence on the dataset used than on the EWI chosen. Generally higher return periods are derived from geostrophic wind than wind gust. An evaluation of the EWIs showed that they could explain between 0 and 50% of the variability of local wind storm return periods obtained from the grid point analysis. The grid point analysis return period estimates are also dependent on the dataset chosen. In particular the advantages of complete coverage given by geostrophic wind speed over wind gust are partially offset by aliasing of the wind extremity due to discrete analysis times, whereas wind gust is an integrated quantity.

Contents

List of Tables

List of Figures

Chapter 1

Introduction

1.1 Project background and literature overview

Accurate knowledge of the frequency distribution of strong surface wind, in particular wind gusts, is of major relevance for insurance related risks in Europe. Reliable climatologies based on in-situ wind observations are almost impossible to obtain as the observations are too coarse in space and/or short and inhomogeneous in time. There are several alternative data sources and analysis techniques that can be used in place of in-situ wind data, each with their own strengths and weaknesses. This study was in part motivated by the needs of the reinsurance industry. In order to estimate the climate impacts of extreme wind events (or any other geophysical extreme event) both in the past and the future, we need an accurate estimate of the magnitude of the extreme wind events as well as their frequency. We take an example from the reinsurance industry, who underwrite the risk of damage caused by strong wind events. A first impression of the vulnerability, or risk, comes from data gathered on the particular impact of interest, in this case high wind induced damage to property, or in monetary terms, loss. The estimates of loss are not representative of the meteorological hazard since loss is affected by many other factors which are non-stationary in time and space. To model loss, it is necessary to have an accurate knowledge of the meteorological hazard itself, including an estimate of the uncertainty. Without accurate knowledge of the hazard risk the best estimate of uncertainty in the risk of loss is not known. In order to obtain accurate information on the magnitude of surface wind during wind storm events the reinsurance company PartnerRe has obtained approximately 100 high resolution dynamically downscaled wind storms from a previous project with MeteoSwiss (Schubiger et al., 2004; Turina et al., 2004). For each wind storm, a modified version of the MeteoSwiss limited area weather forecast model was run using ERA-40 boundary conditions. The high resolution wind storm simulations are ideally suited to the analysis of the local scale wind induced reinsurance losses since they offer a complete spatial coverage of the eastern North Atlantic and western Europe. Another advantage of the high resolution simulations is that the surface wind speeds are similar in magnitude to in-situ measurements (Weisse et al., 2005; Leckebusch et al., 2006; Walser et al., 2006). Therefore, dynamical downscaling can provide more accurate estimates of wind storm magnitude. However, with only a limited number of simulated events, which have been subjectively chosen, accurate determination of the frequency of such events is not possible.

The overall aim of this study is to characterise the climate of extreme winds over Europe and the North Atlantic and to define the return periods (frequency) of some prominent high impact wind storm events. Reinsurance companies often need a singular estimate of the frequency of a wind storm event to estimate the expected frequency of an aggregated loss over a portfolio. Keeping this in mind, and given that the domain of interest is large in scale, we have chosen to use reanalysis data as the basis of this climatology since their is generally a lack of large scale, high temporal and spatial resolution in-situ wind or derived wind datasets available to the climate community for this type of analysis. Reanalysis datasets generated by data assimilation in state of the art global weather forecasting models provide a new source of information for meteorological

statistics (Uppala et al., 2005). Reanalyses provide the temporal extent and homogeneity for comparisons in the frequency domain (e.g. Caires and Sterl, 2005), and the spatial coverage and physical consistency for a continental-scale overview. The quality of reanalyses depends strongly on the parameter, for example, temperature is well captured, even in mountainous areas (Kunz et al., 2007), other parameters like integrated water vapour (Morland et al., 2006) or precipitation might be less realistic in absolute terms. In particular there can be serious biases in absolute wind values (Smits et al., 2005) and in some fields obvious inhomogeneities (Bengtsson et al., 2004; Sterl, 2004; Smits et al., 2005).

Previous studies documenting the extreme wind climate of the North Atlantic and Europe use a number of different data and methodologies depending on the aim of the study. Those aimed at characterising the absolute mean and extreme wind climate at a local level, with or without special attention to time trends have analysed in-situ wind data directly. These studies have had a focus on obtaining the most accurate estimate of return levels (RL), or absolute magnitude of wind or wind gust (Dukes and Palutikof, 1995; Kristensen et al., 1999; Kasperski, 2002; Sacré, 2002; Smits et al., 2005; Bouette et al., 2006; Graybeal, 2006; Walter et al., 2006). Usually, digital access to daily or sub-daily wind measurements on a European scale more than 50 years in length present challenges to using this data (Alexander et al., 2005). Generally it is accepted that in-situ wind data present some serious problems of data homogeneity (although methods exist to correct for exposure, e.g. Verkaik, 2000) and so most studies aimed at determining long term trends and variability have focused on either air pressure observations (Schinke, 1993; Kaas et al., 1996; Alexandersson et al., 1998, 2000; Carretero et al., 1998; Lamb, 1991; Barring and von Storch, 2004; Alexander et al., 2005; Smits et al., 2005), derived wind from air pressure observations (Miller, 2003; Schmith et al., 1998), sea level datasets (e.g. Bijl et al., 1999), derived wind from active and passive microwave sensors aboard satellites (e.g. Monahan, 2006) or use of reanalysis data (Pryor and Barthelmie, 2003; Smits et al., 2005; Weisse et al., 2005; Yan et al., 2002, 2006; Seierstad et al., 2007). A growing number of studies have used high resolution numerical models to downscale global reanalysis data in order to obtain an accurate estimate of wind magnitude (e.g. Turina et al., 2004; Schubiger et al., 2004; Leckebusch et al., 2006; Walser et al., 2006; Walter et al., 2006).

Climate change has promoted a wide study of the potential impacts of the enhanced greenhouse effect on the frequency, duration and intensity of wind storms in a future climate compared to today. Held (1993) provides a good introduction into the response of large scale climate to global warming. In particular, with relation to mid-latitude flow, the opposing effects between changes in the lower tropospheric and mid-tropospheric temperature gradients and the role of increased moisture availability. Recent studies such as Knippertz et al. (2000); Leckebusch et al. (2006); Pinto et al. (2006, 2007); Schwierz et al. (2007) focus on the relationship between the frequency and intensity of cyclones and extreme winds in the present and future climate using a number of GCMs and RCMs. They expect an increase in the both the intensity and the frequency of high wind causing storms over Europe during in the 2071-2100 period compared to today, however this is accompanied by a northward shift of the main North Atlantic storm track (Yin, 2005). Rockel and Woth (2007) for instance show that there is up to a 20% increase in the frequency of extreme winds in the period of 2071-2100 compared to the climate of 1961-1990. Indeed the work of Gillett et al. (2003, 2005) shows that the strengthening of westerlies in the North Atlantic is consistent with anthropogenic climate change over the last 50 years. Other studies show a more muted response of the either the intensity or frequency of cyclones or their affects (such as wave height) in a future climate (Beersma et al., 1997; Carretero et al., 1998; Bengtsson et al., 2006; Pryor et al., 2006).

Thus far convincing observational evidence of an increased intensity of cyclones and their associated surface winds over the North Atlantic and Europe are absent. We therefore approach our task of creating an extreme wind climatology without special attention to long-term non-stationarities. A more detailed literature review on this topic can be found below.

The remainder of the report is divided into four chapters which explain the data and methods

used to determine the return period of high impact wind storms. In the following chapters we present the main results and then conclude with some discussion and recommendations for future research.

Schinke (1993) counted the number of intense cyclones (<990hPa) based on pressure maps and concludes a large increase in the number of severe storms from 1930-1950 and from then on a weakly increasing trend. Due to the subjective nature of the analysis and the change in the amount of data available to weather forecasters who produced the weather maps it is likely that these estimates are flawed. Kaas et al. (1996); Alexandersson et al. (1998); Schmith et al. (1998); Carretero et al. (1998); Bijl et al. (1999); Jones et al. (1999); Alexandersson et al. (2000) using air pressure and sea-level datasets conclude that their has been no change in storminess over the last century, although they note a large positive multi-decadal trend in storminess between 1960 and 1995 associated with a strengthened NAO. However this trend is within the variability of earlier observations. Bhend (2005) used a daily gridded air pressure dataset (Ansell et al., 2006) which extend back to 1850 (Ansell et al., 2006) and applied an objective cyclone tracking algorithm. Using the same North-Atlantic/European domain as Schinke (1993) he shows that the cyclone density is relatively stationary over the period 1880-2003, however this result masks the regional decline in cyclone system density over many ocean areas and increases over land areas. Unfortunately there are still many inhomogeneities in this dataset that preclude more robust findings. Philipp et al. (2006) used the dataset (Ansell et al., 2006) to show that the major winter circulation patterns are stationary during this period. Regionally focused studies such as Schiesser et al. (1997) show a decrease in the frequency of severe storms over Switzerland since around 1880. They used long in-situ data series where the homogeneity was looked at in detail and some corrections were made. Barring and von Storch (2004) used two long term homogenised mean sea level pressure measurements from Lund and Stockholm to define the occurrence of storms since as early as 1780. They conclude that there has been no long term trend in the frequency of occurrence of storminess in the northern part of Europe. Most studies based on the last fifty years of data conclude that their has been an increase in either intensity or frequency of cyclones and associated winds. Miller (2003) note that there is large interdecadal variability in the frequency of severe storms since 1953 and although they do not speculate on a long-term trend, a higher frequency of severe storms is evident in the period from 1980-1995. Alexander et al. (2005) analysed a collection of 21 station based records of sub-daily pressure measurements to define changes in the storm climate of the U.K. and Iceland over the last 45 years. They found a significant increase in the number of severe storms since 1950 in southern U.K. but note that these changes may not be unusual in the context of long term variability. Over The Netherlands Smits et al. (2005) us homogenised daily wind measurements from a number of long records and conclude that the frequency and intensity of extreme winds has decreased over the last 45 years over the Netherlands. This is contrary to results from the NCEP-NCAR reanalysis (Kalnay et al., 1996) which shows an increase in storminess during the same period (Yan et al., 2002, 2006). They conclude that the reason for this discrepancy is likely due to homogeneities in the reanalysis. Pryor and Barthelmie (2003) find an increasing trend in storminess over the Baltic using the NCEP-NCAR reanalysis. Weisse et al. (2005) downscaled NCEP-NCAR using a RCM and found good agreement between modelled wind and observed wind in the North Sea, including a strong upward trend during the period between 1970-1995 consistent with an increasing NAO. In Germany, a high resolution monthly in-situ wind dataset revealed no significant trends over the last 50 year (Walter et al., 2006). Raible (2007) shows that there is no clear trend in the intensity of cyclones over the region during the ERA-40 reanalysis period. It is clear from the literature above that their is no systematic long-term trend in the statistics of wind and their related cyclonic disturbances over the last centuries, a point which is also supported by atmospheric circulation proxy records (Appenzeller et al., 1998; Luterbacher et al., 2002).

Chapter 2

Data and Extreme Wind Indices

2.1 PartnerRe high impact storm catalogue

PartnerRe provided the project with a list of dates of 99 high impact wind storm events over Europe. The dates represent the start date of the regional dynamical model integrations (Schubiger et al., 2004; Turina et al., 2004). The integration start date was chosen such that the integration period of 72 hours would include the period of time when the highest impacts (reinsurance losses) occurred. This date also took into account the need for the regional model to 'spin-up' due to imposed boundary conditions. The list of PartnerRe storm dates are not shown in this document due to their commercial nature.

2.2 ERA-40 data

The ERA-40 reanalysis is 45 years in length and covers the period from September 1957 to August 2002 (Uppala et al., 2005). We focus our results using the data from the extended winter season, October - April since most severe storms have occurred during this season. Of the 99 storms in the PartnerRe dataset 96 occur during the October - April season. For every day there are four reanalysis output times. Given that our study is aimed at extreme winds, we first looked at the wind gust field in ERA-40. Wind gust values represent the maximum wind gust within a six hour period. The data are arranged such that the six hour maximum wind gust is attributed in time to the mid point of each six hour period, i.e. for the 00:00 to 06:00 period the maximum wind gust is written to the time 03:00 value. We also used the 850hPa geopotential field to calculate the geostrophic wind (for reasons of data quality, see below). It is also analysed every 6 hours, however since it is not a maximum value the values are attributed to the times 00:00, 06:00, 12:00 and 18:00.

ERA-40 is a reanalysis dataset, this means that the data consist of a blend between observations and atmospheric and oceanographic model forecast values. As such, no actual observations of wind gust (e.g. as measured from in-situ data) are present in the dataset. The wind gust field is a model forecast value and is based on model parameterisations (see White (2003) for details of the parameterisation method). The geopotential field is an interpolated model field on a constant pressure surface.

The domain we have chosen is based on the domain over which the high resolution model simulations have been made and covers the North Atlantic and European sector from 35° W to 35° E and 35° N to 73° N. The original resolution of the ERA-40 dataset supplied from the ECMWF is roughly 1.125° which has been interpolated to a regular latitude longitude grid with a resolution of 0.5°. This produces a grid of 141 steps in the longitude and 77 steps in the latitude $\rightarrow$ 10857 grid points (gp).

The wind gust at 10m, denoted WG are a function of space and time. A set of observations WG is given by; $WG = \{wg\,(x, y, t) : x = 1, \ldots, n : y = 1, \ldots, m : t = 1, \ldots, k\}$ where $n = 141$,

$m = 77$ and $k = 38204$ and x, y represent the indicial longitude and latitude dimensions.

We also used the geostrophic wind speed calculated from the geopotential height at $850hPa$, Z where $Z = \{z(x, y, t) : x = 1, \ldots, n : y = 1, \ldots, m : t = 1, \ldots, k\}$. The relationship between the geopotential height and geostrophic wind speed is given by equation 2.1 detailed in Holton (2004).

$$\begin{aligned} u_g &= -\frac{g}{f}\frac{\partial Z}{\partial y}, \\ v_g &= \frac{g}{f}\frac{\partial Z}{\partial x} \end{aligned} \tag{2.1}$$

Where u_g and v_g are the y (is real latitude given by the function $latitude(y)$ that maps the indicial y component of the data to the real latitude of the grid point, similarly for $longitude(x)$) and x components of the geostrophic wind (denoted here as y and x for simplicity), g is the acceleration due to gravity at the Earth's surface, f is the Coriolis parameter, $f = 2\Omega \sin(latitude(y))$, Ω is the rotational velocity of the Earth. Taking the scalar of the vector addition of u_g and v_g we derive the geostrophic wind, GW.

To help obtain a better match between the extreme indices defined below and the storm date/time (section 2.1) we converted the reanalysis data into a moving 72 hour maximum wind. Thereby purposely introducing autocorrelation into the data. We used the 72 hour maximum since this is equal to the time over which the maximum wind gust in PartnerRe's high resolution wind fields was calculated.

$wg_{72}(x, y, t) = \max\{wg(x, y, t) : t = t, t + 1, t + 2, \ldots, t + 11\}$ and analogously for gw_{72}. The units of WG, WG_{72} GW and GW_{72} are ms^{-1}. Note that the 72 hour maximum wind datasets were only used for the calculation of the Extreme Wind Indices (EWI, section 2.3) and the Extreme Value Analysis (EVA) of the EWI (section 3). For the grid point analysis the raw 6 hourly values of WG and GW were used for the EVA (section 3). In section 4.3 we estimate the return period (RP) of the wind at each grid point for each catalogue storm. Due to problems matching the exact date/time of the storm at a grid point and the date/time contained within the storm catalogue we calculated the 72 hour maximum wind at each grid point and estimated the RP of this wind using the EVA based on the 6 hourly data (see section 3).

2.2.1 Data inhomogeneities

Initial screening of wind gust data in ERA-40 suggested that in many cases there were unrealistic values over areas of complex orography. Extremely high wind gust values are present in areas of steep orographic gradients compared to the rest of the domain. These areas are almost identical to the areas where the surface roughness, z_0 values are highest in the ERA-40 reanalysis wind gust parameterisation (White, 2003). The roughness length z_0 (figure 2.1) shows a high contrast in values between ocean areas/smooth orography and areas of complex orography such as the Alps and the western coast of Scandinavia.

Surface roughness, z_0 used in ERA-40 over land is a fixed parameter and combines a roughness length derived from land use maps and an extra contribution dependent on the sub-grid scale orography. Over sea z_0 is dependent on the current wind regime in the free atmosphere. The sea surface z_0 becomes higher for high wind regimes and aerodynamically smooth for low wind regimes (White, 2003). The wind gust parameterisation in ERA-40 uses similarity theory and standard approximations which are heavily dependent on z_0. Without delving into the parameterisation process more fully, it is suffice to say that the inclusion of sub-grid scale orography in the calculation of z_0 is having a high practical impact on the realism of wind gusts over complex orography. Note, that the ECMWF has updated the wind gust parameterisation of its operational forecast model in summer 2006. The parameterisation now separates the two contributions to surface roughness resulting in more realistic wind gust values.

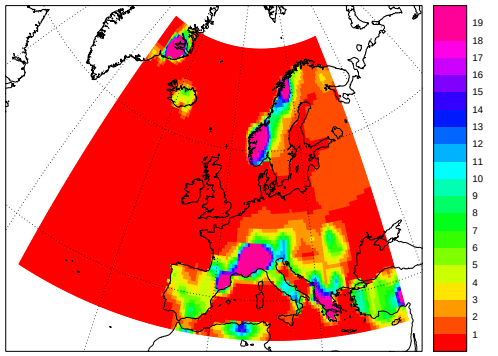

Figure 2.1: The roughness length, z_0 (m) used in the ERA-40 reanalysis dataset (White, 2003; Uppala et al., 2005).

Given these findings, we proceeded by masking these erroneous values. The criteria used to mask a grid point wind gust value is where z_0 is greater than 3 meters and grid points where the elevation of the ERA-40 orography is greater than 700 meters (figure 2.2).

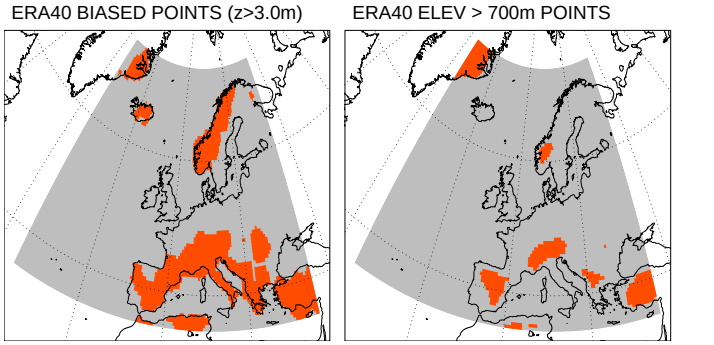

a) b)

Figure 2.2: Areas (grid points shown in red) where WG and WG_{72} from the ERA-40 reanalysis were masked. Surface roughness, z_0 (meters) greater than 3m a) and b) regions where the ERA-40 model orography is greater than 700m.

The selection of these parameters was arbitrarily based on visual inspection of the wind fields during periods of extreme winds. The ERA-40 850hPa geostrophic wind speed values did not show the same biases as the wind gust values (comparing figures 2.3a and c), although there is some influence of mountainous terrain within this dataset. The flow at 850hPa can be seen to accelerate, for example, over the Alps in high wind situations. More discussion on the differences between the data sets and their impact on the results is presented later. Figure 2.3 shows the overall agreement between the ERA-40 data and the high resolution dynamically downscaled wind gust field for a particular storm, Daria (25/02/1990). If we take figure 2.3d as the truth then figure 2.3a clearly demonstrates the need to mask out unrealistic wind gust value over the Alps, coastal Scandinavia and parts of the Mediterranean. There also seems to be some unrealistic values of geostrophic wind in the Alps (figure 2.3c), however these values appear not to be as erroneous as some of the grid points of wind gust.

We also performed a basic check on the temporal homogeneity of the ERA-40 wind values by comparing the mean wind over the domain with the North Atlantic Oscillation Index (NAOI), an index which has been studied widely (e.g. Appenzeller et al., 1998; Wanner et al., 2001; Hurrel

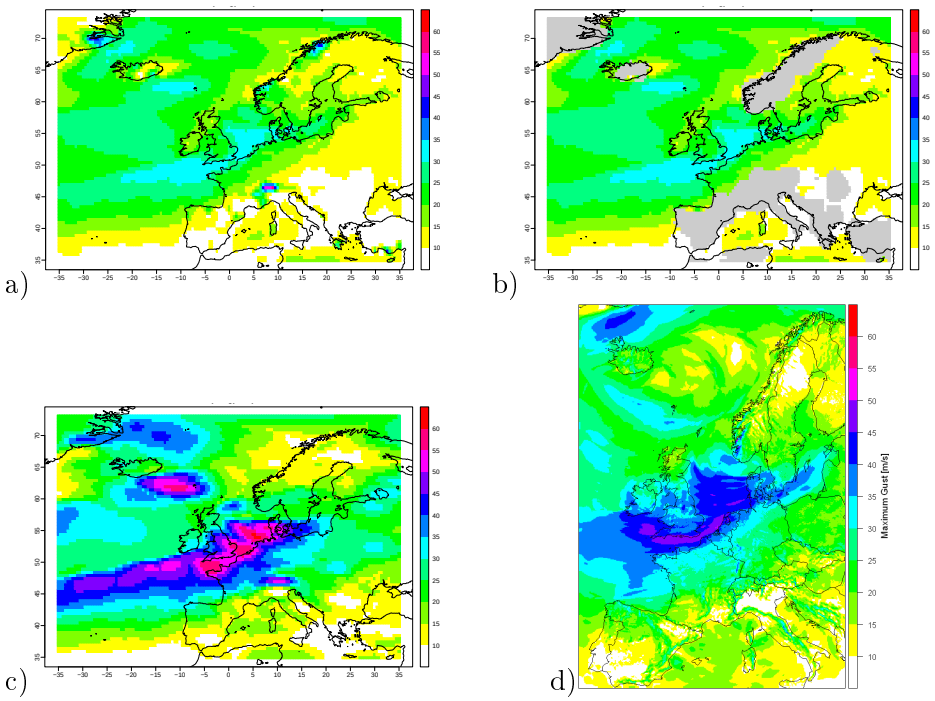

Figure 2.3: A comparison of the 72 hour maximum wind fields using ERA-40 data and the high resolution dynamically downscaled wind gust field for the storm Daria. The ERA-40 wind gust field, WG_{72} unmasked a), b) WG_{72} after masking shown in figure 2.2, c) GW_{72} and d) 72 hour maximum wind gust field from the high resolution dynamically downscaled ERA-40. Note that the projection and scales in a) and b) and c) are different from the scale and projection used in d). All wind values are in m/s.

et al., 2002) and is related to the strength westerlies over the North Atlantic Ocean and Europe.

Figure 2.4 shows a high correlation between the winter NAOI (based on quality controlled and homogenised data) and average wind gust over the whole North Atlantic and European domain considered in this project. The correlation seems to be of a similar strength over the whole period and there appears to be no discontinuities in the series. We considered this to be a very general indicator of temporal homogeneity in the ERA-40 wind data.

2.3 Derived extreme wind indices

Scalar indices have been used to summarise a wind storm's magnitude and spatial extent. Reinsurance companies often need a singular estimate of the frequency of a wind storm event to estimate the expected frequency of an aggregated loss over a portfolio. In other words they need a frequency estimate of the wind storm event and not only the frequency (return period) of wind speed (or wind gust) at a specific place. A number of such different compound extreme wind indices were previously analysed by PartnerRe which we used as a basis for the different indices presented below. In this report we only present a selected number of such indices which we determined to be independent enough and useful in the assessment of the RPs. More details about the extreme wind indices (EWI) are found below and we demonstrate their performance in the results section 4.

2.3.1 Domain specification

Since the PartnerRe storm catalogue was chosen with respect to wind storms which affected mainly land areas of Europe we decided to investigate the effect of using various sub domains within the main North Atlantic - European domain as specified in section 2.2 over

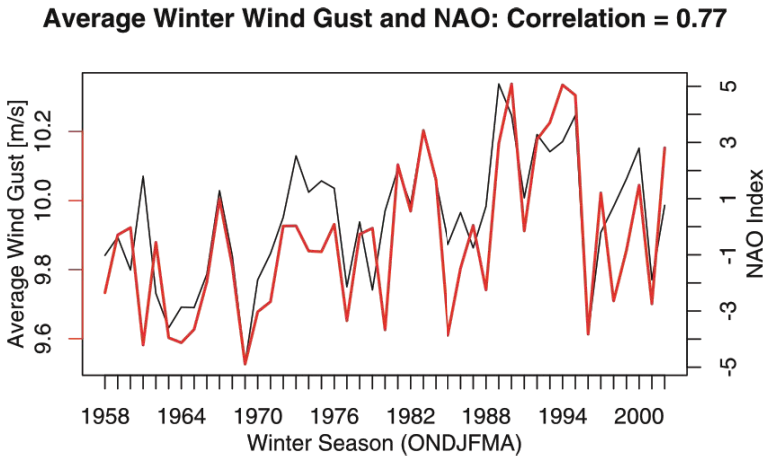

Figure 2.4: Time series of mean WG over the domain (red line) using ERA-40 data and the NAOI index (black line) from 1958-2002. The NAOI used was from Hurrel et al. (2002).

which to calculate the extreme indices. The specification of various sub domains in space is given by Δ_δ where Δ specifies a geographical domain which is dependent on δ, the type of mask applied to the data. The variations in the term δ are explained in table 2.1. Where $\delta \in \{all, land, sea, all-unreal, land-masked, sea-masked\}$, i.e. there are 6 different sub domains.

Symbol	Applied Masks	Description
Δ_{all}:	Raw	All grid points in the domain 35° W - 35° E and 35° N - 73° N
Δ_{land}:	Land only	All grid points over land within 35° W - 35° E and 35° N - 73° N
Δ_{sea}:	Sea only	All grid points over sea within 35° W - 35° E and 35° N - 73° N
$\Delta_{all-masked}$:	Masked unrealistic grid points	All grid points in the domain not identified as being erroneous as shown by figure 2.2
$\Delta_{land-masked}$:	Land only and masked unrealistic grid points	Combinations of masks 2 and 4
$\Delta_{sea-masked}$:	Sea only and masked unrealistic grid points	Combination of masks 3 and 4

Table 2.1: Definition of sub domains, Δ_δ .

2.3.2 Extreme wind indices

The following indices are denoted in terms of a generic wind variable, W and could be substituted for either WG_{72} or GW_{72} defined above. Where possible we tried to take into account the unequal areas of each grid box by weighting of sums and multipliers by the cosine of the latitude of each grid point. For each index we provide a brief rationale and their expected sensitivity.

$\bar{X}$: Mean wind. This index is simply a weighted mean of wind speed over a given area. The index is likely to be sensitive to both the severity of the wind storm and its spatial extent.

$$\bar{X}(t) = \frac{1}{N_{\kappa\delta}} \sum_{x,y \in \Delta_\delta} \kappa(x,y)\, w(x,y,t) \tag{2.2}$$

where κ are the individual grid point weights which only depend on y, $\kappa(x,y) = \cos(latitude(y))$, $N_{\kappa\delta} = \sum_{x,y \in \Delta_\delta} \kappa(x,y)$ and Δ_δ denotes the domain.

$Q95$: **The spatial 95% quantile wind.** This index is aimed at measuring the lower bound of wind speed in the top 5% of the area considered and is therefore more likely to be an estimate of storm severity than $\bar{X}$.

$$Q95(t) = F_*^{-1}(p) = \min\{w : p \leq F_*(W)\} \tag{2.3}$$

where $p = 0.95$ and F_* is the latitude weighted empirical cumulative distribution function of $\{w(x,y,t) : (x,y) \in \Delta_\delta\}$ where Δ_δ denotes the domain. The weighted cumulative distribution function is given by equation 2.4 (Horvitz and Thompson, 1952; Research Triangle Institute, 2001).

$$F_*(W) = \frac{1}{N_{\kappa\delta}} \sum_{x,y \in \Delta_\delta} \kappa(x,y) \mathbb{1}(w(x,y,t) \leq W) \tag{2.4}$$

Where κ are the individual grid point weights and $N_{\kappa\delta}$ is given above and $\mathbb{1} = \begin{cases} 1 : w(x,y,t) \leq W \\ 0 : otherwise \end{cases}$.

$SQ95$: **Sum of all wind above the spatial 95% quantile.** This index is expected to be sensitive to the range of wind speeds in the top 5% of the area considered. However, it is shown later in the results section that this index has relatively little variability and is not sensitive to the storm events considered.

$$SQ95(t) = \sum_{x,y \in \Delta_\delta} \mathbb{1}_{\{>Q95(t)\}} (\kappa(x,y) w(x,y,t)) \kappa(x,y) w(x,y,t) \tag{2.5}$$

where $\mathbb{1}_{\{>Q95(t)\}} = \begin{cases} 1 : \kappa(x,y) w(x,y,t) > Q95(t) \\ 0 : otherwise \end{cases}$.

$Sfq95$: **Sum of the fraction of wind divided by the grid point 95% quantile.** It was envisaged that this index summarise the extremity of the wind over a given area relative to the local extreme wind climate at each grid point. For this we have calculated the local wind percentiles denoted q.

$$Sfq95(t) = \sum_{x,y \in \Delta_\delta} \mathbb{1}_{\{>1\}} \left(\frac{w(x,y,t)}{q95(x,y)} \right) \cdot \kappa(x,y) \frac{w(x,y,t)}{q95(x,y)} \tag{2.6}$$

where κ are the weights given above, the $\mathbb{1}_{\{>1\}} = \begin{cases} 1 : \left(\frac{w(x,y,t)}{q95(x,y)}\right) > 1 \\ 0 : otherwise \end{cases}$. The grid point quantile function $q95$ is given by:

$$q95(x,y) = F^{-1}(p) = \min\{w : p \leq F(W)\} \tag{2.7}$$

where $p = 0.95$, F is the empirical cumulative distribution function of $\{w(x,y,t) : t \in ONDJFMA\}$

$Sfq95q99$: **Sum of the fraction of extreme wind divided by the length of the distribution tail.** This index should also be sensitive to the relative extremity of local wind speed, however, unlike $Sfq95$ this index has a normalising factor which is proportional to the length of the tail of the local extreme wind distribution. This index should give equal weight to the winds in a storm region whether the storm be located over the sea or land, where we see a contrast in both the scale and shape of the local extreme wind distribution (see figure 4.15c and d)

$$Sfq95q99(t) = \sum_{x,y \in \Delta_\delta} \mathbb{1}_{\{>0\}} \left(\frac{w(x,y,t) - q95(x,y)}{q99(x,y) - q95(x,y)} \right) \cdot \kappa(x,y) \frac{w(x,y,t) - q95(x,y)}{q99(x,y) - q95(x,y)} \tag{2.8}$$

where κ are the weights given above, the $\mathbb{1}_{\{>0\}} = \begin{cases} 1 : \left(\frac{w(x,y,t)-q95(x,y)}{q99(x,y)-q95(x,y)}\right) > 0 \\ 0 : otherwise \end{cases}$. The grid point quantile functions, $q95$ and $q99$ are given above.

Chapter 3

Extreme Value Analysis

3.1 The generalised Pareto distribution

It is often the case that when quantifying extremes of any physical process there are limited observations of such a process. Usually, from an application point of view, we require information about extremes which have not been observed. This requires extrapolation of information from the observations at hand. Techniques based on the asymptotic behaviour of observed extremes form the basis of EVA (Fisher and Tippett, 1928; Coles, 2001). Palutikof et al. (1999) review common methods used to estimate the extreme value distribution of extreme wind speeds. Generally it is accepted that the Peaks Over Threshold (POT) method is preferable to a classical Generalised Extreme Value (GEV) modeling of annual maxima (Brabson and Palutikof, 2000). This is due to the fact that the former uses more of the available data to fit a model, generally leading to a better characterisation of the extreme part of the parent distribution. However, with the use of the POT method comes the necessity to insure that the data are i.i.d. (independent and identically distributed). The most prevalent form of non-stationary in wind data is temporal and spatial autocorrelation. The time non-stationarity is usually addressed by some form of declustering technique that insures temporal independence in the extreme events. The issue of spatial autocorrelation is a complex, rather new and growing field which is beyond the scope of the present study to address appropriately (Coles, 2001). In any case, the ignorance of spatial autocorrelation means that we should adopt a conservative attitude to the uncertainty estimates we present for the RPs and RLs. Another key criteria for the use of the POT series is the selection of the threshold over which the extreme value distribution model is fitted. Our approach to these two key problems are outlined below, however, first we introduce the Generalised Pareto Distribution (GPD), the distribution which will be used to model the POT series.

Following Coles (2001) the GPD can be written in terms of a generic variable x as:

$$G(x) = 1 - \left[1 + \frac{\xi}{\sigma}(x - u)\right]^{-\frac{1}{\xi}} \tag{3.1}$$

Conditional on $x > u$ and $\xi \neq 0$ where u is the selected threshold. The GPD is characterised by two parameters, ξ the shape parameter and σ the scale parameter. If $\xi > 0$ then the maximum of the GPD is unbounded, whereas if $\xi < 0$ then the tail has a finite extent, if $\xi = 0$ then the GPD reduces to the exponential distribution and is also unbounded in the limit $\xi \to 0$. Equation 3.1 can be rewritten in terms of probabilities:

$$\Pr(X > x) = \zeta_u \left[1 + \xi\left(\frac{x - u}{\sigma}\right)\right]^{-\frac{1}{\xi}} \tag{3.2}$$

where $\zeta_u = \Pr(X > u)$ i.e. ζ_u is the probability of the occurrence of an exceedance of a high threshold, u. In this study we are primarily interested in the the N-year return level (RL), x_N

which is exceeded once every N years and is the solution of,

$$\zeta_u \left[1 + \xi \left(\frac{x_N - u}{\sigma}\right)\right]^{-\frac{1}{\xi}} = \frac{1}{N n_y} \tag{3.3}$$

Rearranging,

$$x_N = u + \frac{\sigma}{\xi}\left[(N n_y \zeta_u)^{\xi} - 1\right] \tag{3.4}$$

where n_y is the number of observations in each extended winter season. Equation 3.4 suggests that in order to determine the N-year RL three parameters need to be fitted, ξ, σ and ζ_u. If we assume that these are rare events ζ_u could be expected to follow a Poisson distribution. Here we deviate slightly from Coles (2001) who suggests ζ_u could be modelled by the binomial distribution. The Poisson distribution is characterised by λ, the mean number of threshold exceedances per unit time. We can estimate $\zeta_u \approx \lambda / n_y$ and reformulating equation 3.4 in terms of the λ (as also shown by Palutikof et al., 1999) we get:

$$x_N = u + \frac{\sigma}{\xi}\left[1 - (\lambda N)^{-\xi}\right] \tag{3.5}$$

We estimated ξ , σ and λ in equation 3.5 using maximum likelihood (ML) (Martins and Stedinger, 2000; Coles, 2001). The form of the negative log likelihood function which we minimised (assuming $\xi \neq 0$, modified accordingly when $\xi = 0$) is given by equation 3.6.

$$\ell(\lambda, \sigma, \xi) = -\log\left(\frac{e^{-\lambda\eta}\lambda\eta^{\eta}}{\eta!}\right) + k\log\sigma + \left(1 - \frac{1}{\xi}\right)\sum_{t=1}^{k}\log\left(1 - \xi\left(\frac{x_t - u}{\sigma}\right)\right) \tag{3.6}$$

where η is the number extended winter seasons in the dataset (45 in the case of the ERA-40 data). In practice the solution of the first term in 3.6 is solved using a truncated version of the Poisson distribution (Ahrens and Dieter, 1982).

3.2 Declustering and threshold selection

In order to satisfy the GPD model requirements of independent extreme events it is necessary to decluster the time series. Extreme winds during the winter over Europe are associated with mesoscale and synoptic scale cyclones (Wernli et al., 2002). Typically these systems have a lifetime of around 72 hours or less. Since the time resolution of our data is as low as 6 hours the time series of extreme indices and the grid point winds are expected to display a high amount of autocorrelation. This is confirmed by the analysis of the partial autocorrelation function (not shown). Typical methods to help make extremes in the POT series independent are given in Coles (2001). Most methods used to decluster a time series are based on the estimation of a statistic called the extremal index, θ. In the presence of no autocorrelation (clustering) in the series then $\theta = 1$ else if $\theta < 1$ then there is clustering in the data. The closer θ is to zero the greater the clustering observed in the series. The extremal index can be thought of as the reciprocal of the limiting mean cluster size (Coles, 2001).

There have been a number of estimates of θ proposed in the literature, we chose the estimator of Ferro and Segers (2003) since they show that their estimate has better declustering characteristics than other commonly used methods of estimating θ. Their method has the advantage that it is *automatic* in the sense that θ changes with the given threshold, u. The extremal index, θ given by Ferro and Segers (2003) is based on the inter-exceedance times, T. Firstly we define N, the number of values in a series W which exceed the threshold u.

$$N = \sum_{t=1}^{k} \mathbb{1}_{\{>u\}}(w(t)) \tag{3.7}$$

where $\mathbb{1}_{\{>u\}}(w(t)) = \begin{cases} 1 & \text{if } w(t) \geq u \\ 0 & \text{if } w(t) < u \end{cases}$. Let $1 \leq S(1) < \ldots < S(N) \leq k$ be the exceedance times. Then the observed inter-exceedance times are $T(i) = S(i+1) - S(i)$ for $i = 1, \ldots, N-1$. The extremal index, θ is defined in terms of u and T by the following expressions.

$$\tilde{\theta}(u) = \begin{cases} 1 \wedge \hat{\theta}(u) & \text{if } \max\{T(i) : 1 \leq i \leq N-1\} \leq 2 \\ 1 \wedge \hat{\theta}^*(u) & \text{if } \max\{T(i) : 1 \leq i \leq N-1\} > 2 \end{cases} \tag{3.8}$$

where $\hat{\theta}(u)$ and $\hat{\theta}^*(u)$ are given by:

$$\hat{\theta}(u) = \frac{2\left(\sum_{i=1}^{N-1} T(i)\right)^2}{(N-1)\sum_{i=1}^{N-1} T(i)^2} \tag{3.9}$$

$$\hat{\theta}^*(u) = \frac{2\left(\sum_{i=1}^{N-1} (T(i)-1)\right)^2}{(N-1)\sum_{i=1}^{N-1} (T(i)-1)(T(i)-2)} \tag{3.10}$$

The expressions above give us an estimate of θ which are based on inter-exceedance times T. A reason for using the method of Ferro and Segers (2003) is that their estimate of $\tilde{\theta}$ is shown to be a better estimate of the the true value of θ than the commonly used *runs declustering* estimator for thresholds, u in the range of $F(w) < 0.95$. The extremal index in this case is the proportion of inter-exceedance times that may be regarded as inter-cluster times (Ferro and Segers, 2003). To arrive at a declustered series we can assume that the number of independent clusters is given by $n_c = 1 + \lfloor \theta N \rfloor$. Now we find the jth ordered inter-exceedance time, r and find the cumulative sum of inter-exceedance times that are greater than r, this gives us a series of inter-exceedance times which belong to each cluster.

Ferro and Segers (2003) show that their estimate of θ is only representative if it is calculated on a strictly stationary series. Since we have based our investigation on the extended winter season (October-April) our time series have a pronounced seasonal cycle in them. Analyses showed that the performance of the declustering method was degraded. In order to compensate for this we removed the seasonal cycle by only considering a POT series where the threshold varied over the season. We defined a daily threshold, $u(t)$ corresponding to the daily 90th percentile. The daily percentile was calculated from 180 values; four observations per day (6 hourly intervals) over 45 years of the ERA-40 period. An example is given in Figure 3.1.

Note that the daily 90th percentile series is quite noisy, likely due to sampling, therefore we used a smoothing spline to make an estimate of the true climatology. It is important to note that the daily threshold, $u(t)$ was only used to help the declustering procedure to obtain the POT series, in the GPD analysis we still used a fixed, non-seasonally varying, threshold u.

An example of the performance of the declustering method for the extended winter seasons of 1989/90 and 1999/2000 are given in Figure 3.2. From figure 3.2a it can be seen that the declustering method is working very well, separating the two well known wind storms of that season, Daria and Vivian into separate clusters (storms from storm catalogue are shown as red vertical lines). However, note that both Vivian and Wiebke belong to the same cluster (light blue) where as a number of other lower intensity events, such as Herta have a separate cluster.

Figure 3.2b shows the performance of the declustering method during the season of 1999/2000. The wind storm Anatol is clearly separated in its own cluster, whereas the storms Lothar and Martin are within the same cluster. This highlights one of the limitations of the extreme indices approach and the underlying reanalysis data. The index and hence the declustering method cannot differentiate between the two storms Lothar and Martin.

As a comparison we also applied the *runs declustering* (Coles, 2001) method and note that sometimes the GPD model of the POT series appears to fit the data better (in terms of quantile-quantile plots, example shown below, see also figure 4.6), however the choice between the Ferro

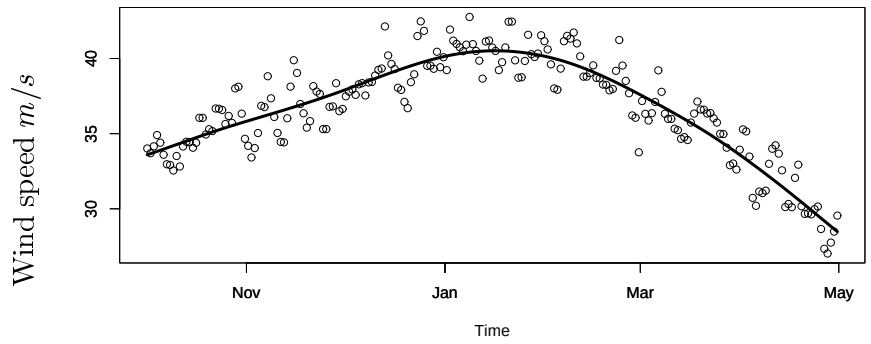

Figure 3.1: An example of the fitted (thick black line) daily 90th percentile threshold (open black circles) from the $Q95$, GW_{72} , Δ_{all} (see table 2.1) index used to create a POT series on which the declustering method of Ferro and Segers (2003) was applied for the ONDJFMA season. Each daily empirical 90% quantile was calculated from approximately 180 values (45 years $\times 4$ observations per day). The smooth curve was fitted using a cubic spline where the smoothing parameter was set to a arbitrary value to obtain a smooth seasonal cycle.

and Segers approach or runs declustering seemed to have little practical influence on the return period results (see figure 4.6).

We used a number of different diagnostics to help choose a fixed threshold over which the declustered POT series is modelled by the GPD (Equation 3.1). The two plots in figure 3.3 show the modified scale and shape as a function of threshold, u according to the methods in Coles (2001) for the extreme index $Q95$. According to the postulates of the GPD, both the modified scale parameter and the shape parameter should be invariant with threshold.

From the figure 3.3 we can see that almost all thresholds are suitable given the large uncertainty in the estimates of both the modified scale and the shape parameter. In these examples the tested threshold only goes as low as the 90th percentile, however other similar plots which go back as far as the 70th and 80th percentile show nonlinearity. Based on a number of these plots for different indices and different datasets (WG_{72} and GW_{72}) we decided to take the seasonal (ONDJFMA) 90th percentile as the threshold above which we create the POT series and subsequently model with the GPD. This threshold was chosen as low as possible to enable as many catalogue storms to be above the threshold and still satisfy the requirements of the GPD.

Figure 3.4 demonstrates that the GPD fit to the Ferro and Segers (2003) daily declustered $Q95$, GW_{72} for the region Δ_{all} is a good fit to the data. Other examples of the quality of the GPD fits are shown in figures 4.4 and 4.14.

For the grid point analysis we used WG and GW which are resolved every 6 hours and have not been converted into a 72 hour maximum. One of the reasons we wished to perform the grid point analysis on these data was to avoid introducing autocorrelation into the data for the purpose of matching the ERA-40 data with the storm catalogue when it was not needed.

An immediate difference in the grid point POT series (figure 3.5) is the lack of autocorrelation compared to the extreme index POT as shown in figure 3.2. The examples for two grid points, one in the north of the British Isle's and the other in the north east of Europe, for the same season (1999/2000) show very different wind values and clustering. For the same season there are many more POT identified by the grid point winds than the $Q95$ index (figure 3.2b). We think that this is one of the advantages of the grid point analysis since the extreme value modelling is relative to the local climatology. For comparison purposes we also show the dates of the storms in the storm catalogue (vertical red lines). We note that the coincidence between the peaks of the clusters and the storm dates seldom match in the grid point analysis. This is not surprising given the way the storm dates have been constructed. After the analysis of many diagnostics

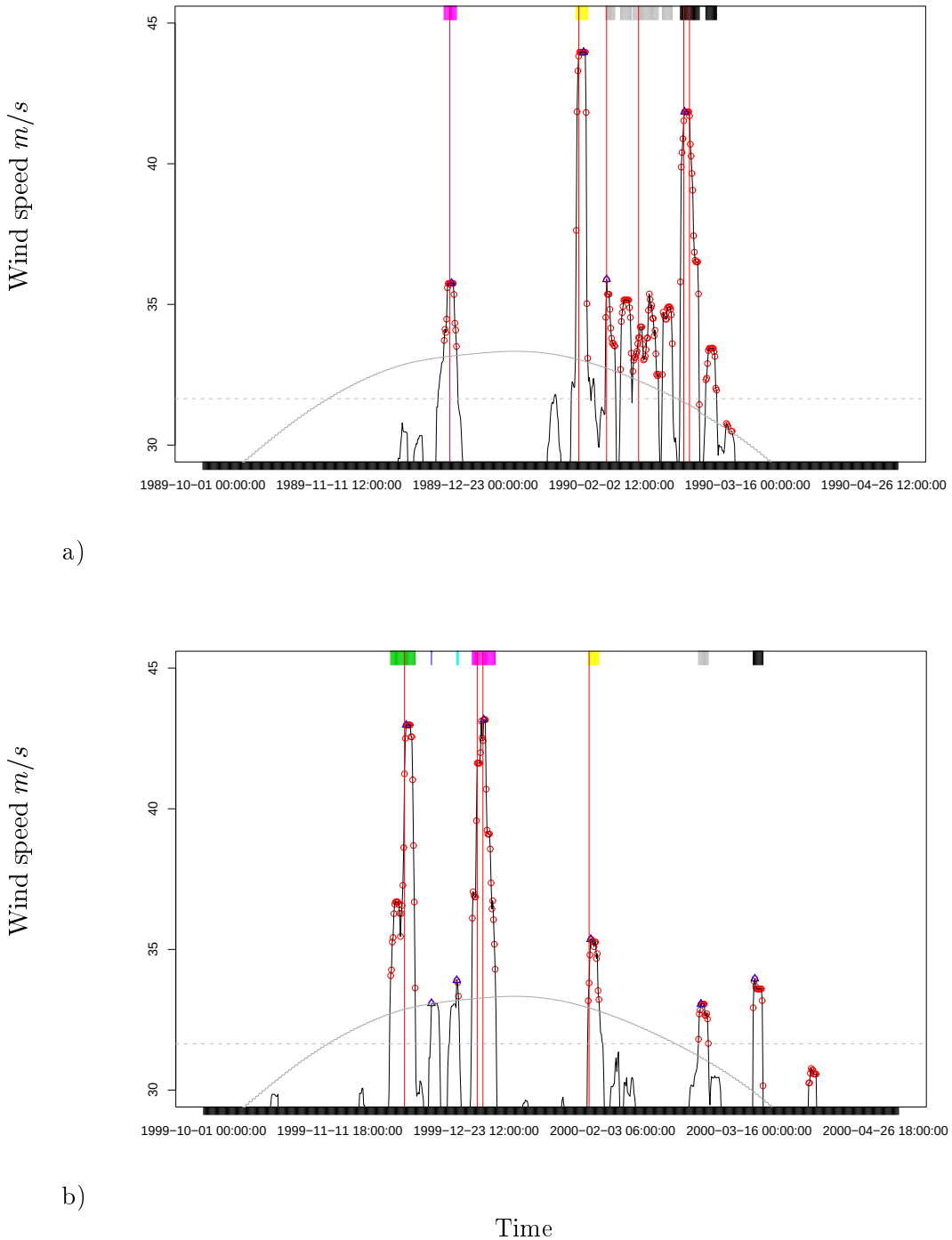

Figure 3.2: Examples of a daily declustered POT series using the approach of Ferro and Segers (2003) for the extended winter season (ONDJFMA) of 1989/90 a) and b) 1999/2000. The thin black line is the $Q95$ index calculated over the land only (Δ_{land}) using GW_{72}. The red circles indicate values of the index which exceed the daily threshold (not shown). Blue triangles show the maximum value of the index within each cluster. Membership of POTs (red circles) to a particular cluster are denoted by colored bands on the top margin of the plot. The solid and dashed grey lines show the daily 90th percentile and the seasonal 90th percentile respectively. The vertical red lines indicate the date of the storms in the storm catalogue, with the names (from left to right, i.e. start of the season to the end of the season) in a) unknown name, Daria, Herta, Nana, Vivian and Wiebke and in b) Anatol, Lothar, Martin and Kerstin.

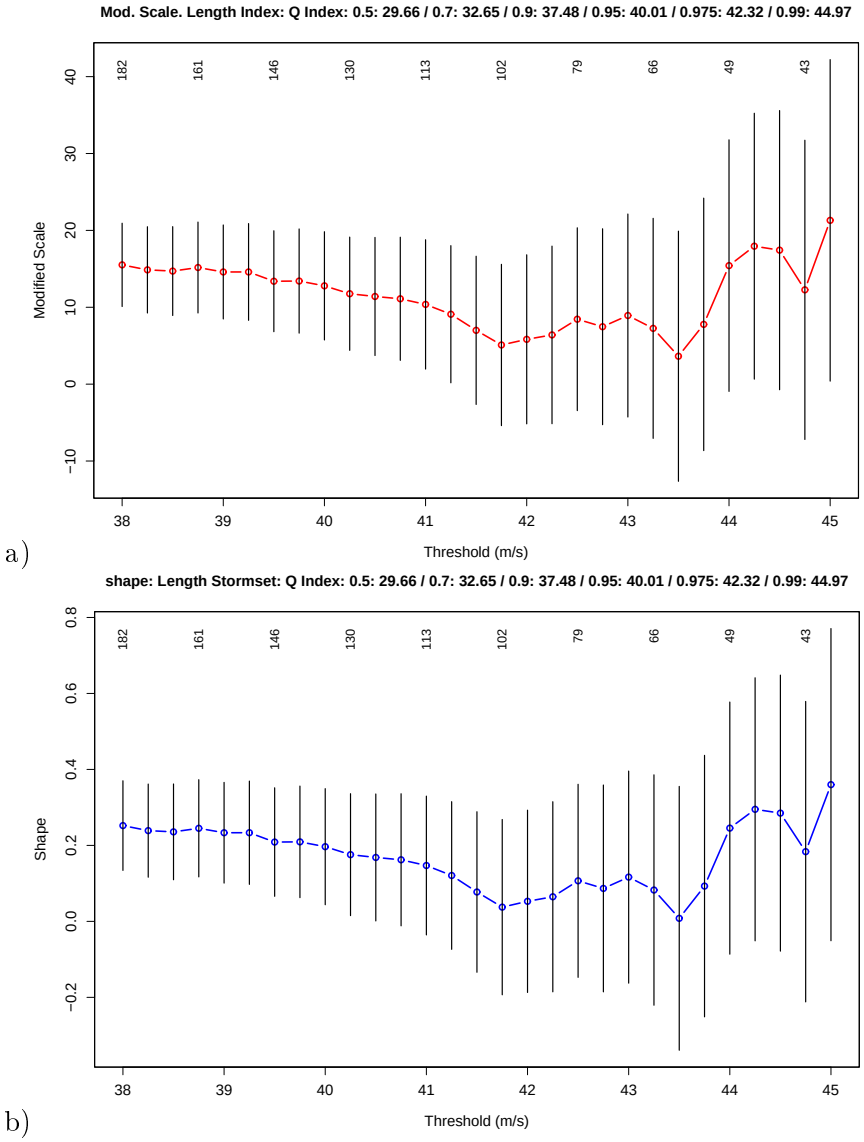

Figure 3.3: Modified Scale, $\sigma*$ a) (see Coles, 2001) and the negative shape, $-\xi$, b) parameter diagnostic plots for selecting the fixed threshold above which the declustered POT will be modelled using the GPD. This example is based on the declustered POT $Q95$, GW_{72} for the region Δ_{all}. The vertical black lines denote the 95% confidence intervals calculated using the parametric resampling technique detailed in section 3.3. The numbers aligned vertically in the top of the plot are the number of cluster maxima identified by the declustering technique. The numbers in the header of each plot show the empirical quantile value at various cumulative probabilities from 0.9 to 0.99.

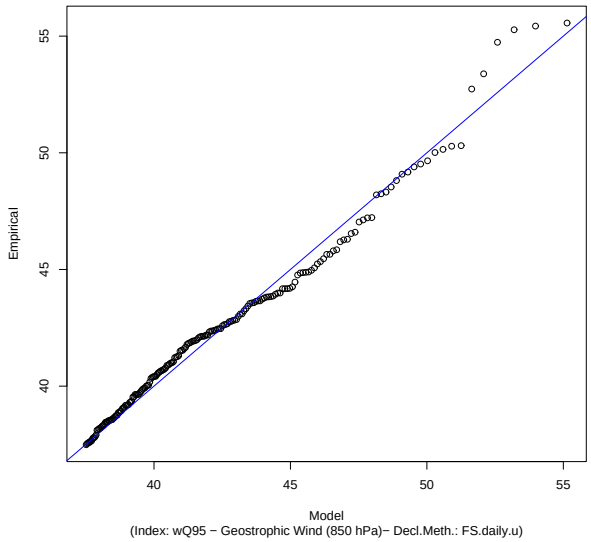

Figure 3.4: A quantile-quantile (qq) plot (m/s) of the fitted GPD to the declustered $Q95$, GW_{72} for the region Δ_{all}.

plots for many different grid points it became clear that we needed to choose a higher threshold than that chosen for the EWIs. In many cases choosing the 95th percentile gave good results in terms of the GPD fit. See figure 3.6 for threshold diagnostics and figure 4.14 for quantile-quantile plots.

3.3 Uncertainty calculations

Three different methods of calculating uncertainty of RPs and RLs were intercompared. The first of these methods is called the *delta method* (Coles, 2001) and is based on the assumption that the maximum likelihood estimates (MLE) of the parameters of the GPD are modelled by a multivariate normal distribution (Coles, 2001). The method finds the inverse of the observed information matrix and is multiplied by the standard normal variate to form confidence intervals on parameters of the GPD or scalar functions of the parameters such as x_N. The observed information matrix is the curvature of the log likelihood surface based on observations, to obtain this matrix we take the gradient vector given by the equation below.

$$\nabla x_N^T = \left[\frac{\partial x_N}{\partial \lambda}, \frac{\partial x_N}{\partial \sigma}, \frac{\partial x_N}{\partial \xi}\right] \tag{3.11}$$

and use the MLE variance-covariance matrix, V such that the $Var(x_N) \approx \nabla x_N^T V \nabla x_N$ where the superscript T denotes the transpose of the matrix. We improved the calculation of the delta method by explicitly solving the partial derivatives compared to the routines provided in Coles *evd* R package which uses first differences. One immediate drawback of this method is that the uncertainty estimates are constrained to be symmetrical, which in the case of uncertainty in RPs may not be physically meaningful.

The second method we use is a *parametric resampling technique*. In this method we start by generating a random number of threshold exceedances by assuming a Poisson process and using the length of the POT series as the average number of occurrences of a POT, n. We then produce n samples from the uniform distribution and use these together with the ML fitted values (from the real observations) of ξ , σ and the fixed value of u to generate a random POT series using the GPD quantile function (the inverse of equation 3.1). The next step is to fit a GPD to this random POT series. This method is repeated a large number of times in order to build a sampling distribution for the GPD parameters and hence x_N on which empirical estimates of the

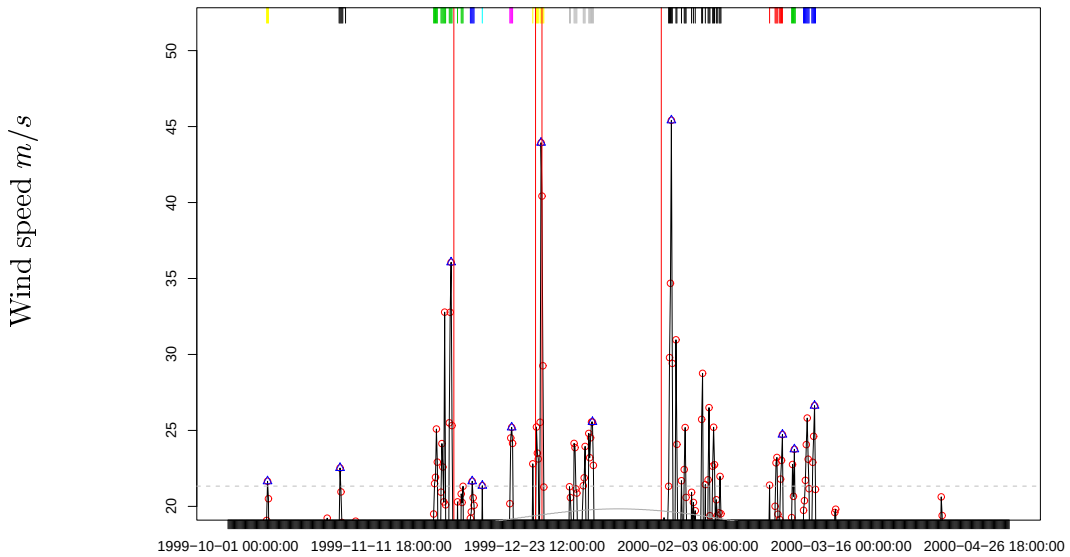

a)

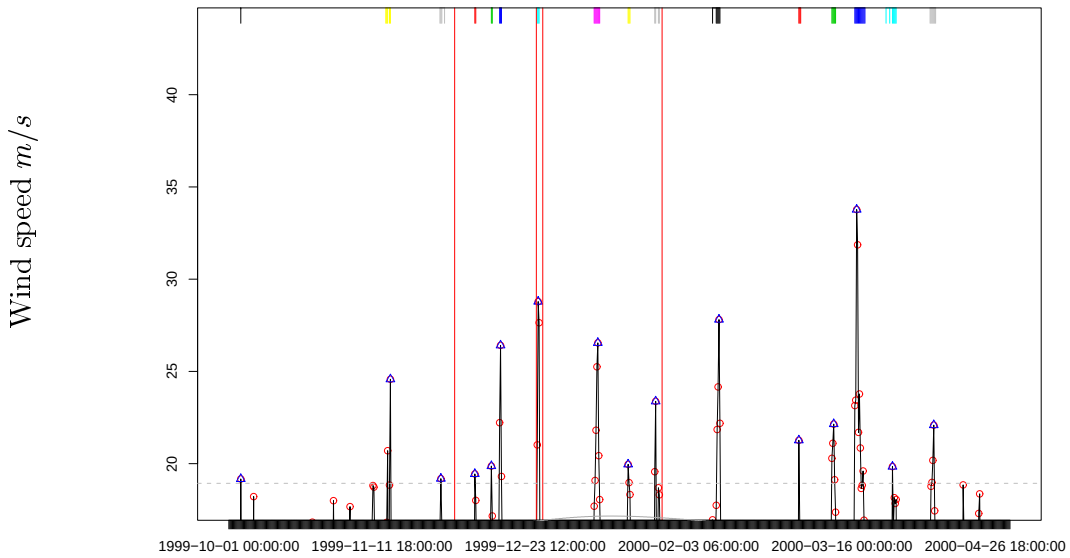

b)

Time

Figure 3.5: An example of a daily declustered POT series using the approach of Ferro and Segers (2003) for the grid points 2.5° W, 57° N a) and b) 30° E, 67° N. The thin black line is the *GW* during the extended winter season (ONDJFMA) of 1999/2000. The red circles indicate values of the index which exceed the daily threshold (not shown). Blue triangles show the maximum value of the wind within each cluster. Membership of POTs (red circles) to a particular cluster are denoted by the colored bands on the top margin of the plot. The solid and dashed grey lines show the daily 90th percentile and the seasonal 90th percentile respectively. The vertical red lines indicate the date of the storms in the storm storm catalogue, with the names, Anatol, Lothar, Martin and Kerstin.

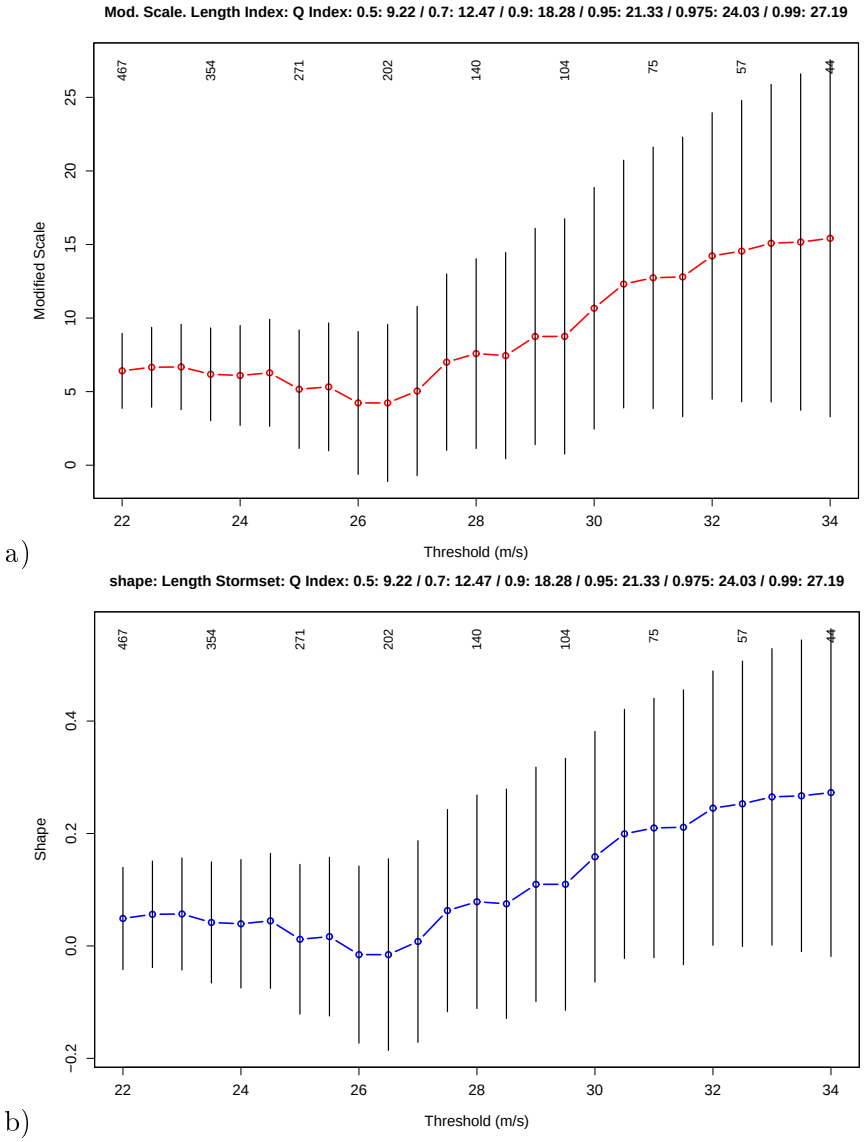

Figure 3.6: Modified Scale, $\sigma*$ a) (see Coles (2001)) and the negative shape, $-\xi$, b) parameter diagnostic plots for selecting the fixed threshold above which the declustered POT will be modelled using the GPD. This example is based on the declustered POT *GW* for the grid point 2.5° W, 57° N. The vertical black lines denote the 95% confidence intervals calculated using the parametric resampling technique detailed in section 3.3. The numbers aligned vertically in the top of the plot are the number of cluster maxima identified by the declustering technique. The numbers in the header of each plot show the empirical quantile value at various cumulative probabilities from 0.95 to 0.99.

confidence intervals are constructed. The parametric resampling technique is an improvement on the delta method primarily because the method allows non-symmetric uncertainty estimates of RPs since it is not constrained by the multivariate normality assumption of the MLEs. The method is still parametric since it is dependent on the Poisson sampling of the POT series, however this method is intuitively appealing since we are quantifying the effect of resampling the frequency of occurrence, the parameter that we are most interested in.

The third method we use is *profile log-likelihood*. It has the advantage over the other two methods in that it utilises more information from the sample, especially the information provided by the most extreme events. Using this method it is also possible to obtain asymmetric uncertainty estimates which according to Coles (2001) are more accurate and should be used in situations where it is necessary to obtain accurate confidence intervals. Since a major aim of this study is to obtain accurate confidence intervals on the RP estimates we think it is prudent to use this method. For each parameter the profile log-likelihood method maps the log likelihood surface of one parameter while keeping the other parameters fixed at their maximum likelihood values. In this way a likelihood profile surface can be be evaluated close to the maximum likelihood estimate of each parameter and/or derived parameters such as x_N. Following Coles (2001) the profile log likelihood method can be summarised by the following equation, in this case the profile of x_N the RL for a given RP, N, and is similarly arranged for determining the profile of other parameters;

$$\ell_p(x_N) = \max_{(\lambda,\sigma,\xi)} \ell(x_N, (\lambda, \sigma, \xi)) \tag{3.12}$$

Equation 3.12 determines the profile, however, to determine the confidence interval width Coles (2001) makes use of the deviance statistic which is approximately chi-square distributed.

$$D_p(x_N) = 2\{\ell(x_N, \lambda, \sigma, \xi) - \ell_p(x_N)\} \sim \chi^2_1 \tag{3.13}$$

Figure 3.7 compares the three different methods of calculating uncertainty of the RL and RPs using an extreme value index and choosing the 95% confidence interval. Unlike the parametric resampling and the delta method, the profile log-likelihood method gives a more bounded upper limit which only tends to infinity for much higher than observed RLs/RPs. The profile log-likelihood method is capturing the apparent non symmetrical nature of the uncertainty in the GPD fit (green curve is symmetrical in RL and in RP, note the log scale). Physically we do not expect the upper bound of uncertainty to be infinite for high RLs/periods since the amount of energy and hence wind speed produced by cyclones is limited, therefore we have more confidence in the uncertainty estimates of the profile log-likelihood method.

We used the profile log-likelihood method for all the following analyses and results. However, since there is no analytical solution that describes the log-likelihood profile, the method involves sampling a number points on the profile and then fitting a spline to the fitted points in order to obtain a more continuous profile. Due to smoothness constraints of the spline and computational considerations, the uncertainty calculations for RPs less than 0.3 years were unreliable. In these cases we simply substituted the uncertainty calculated from the maximum likelihood variance of the mean peak over threshold occurrence per season, λ and used the approximate normality (as in the delta method) of the MLE to construct a confidence interval. While this method usually resulted in wider confidence intervals than the uncertainty estimates with RPs above 0.3 years, we considered this acceptable given the problems with the profile method. Another example of where we use this methodology is when a catalogue storm is not sufficiently high enough in magnitude to be above the GPD threshold. In this case we estimated the RP to be $1/\lambda$.

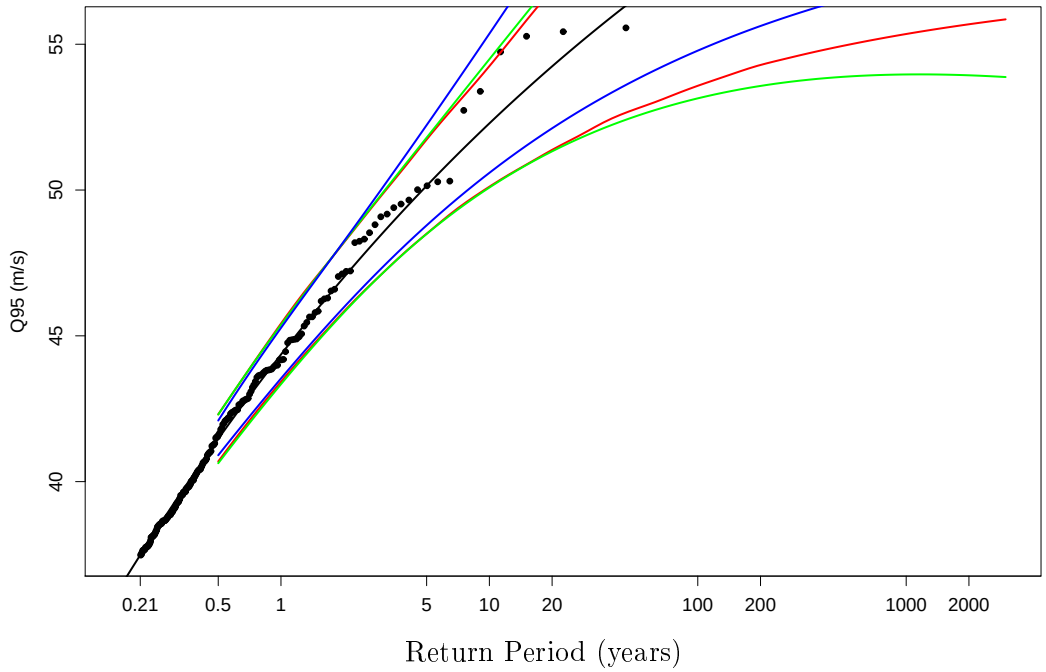

Figure 3.7: A comparison of the various methods used to calculate the uncertainty in the estimates of the RP (years) and RL (m/s). The example uses the GPD fit to $Q95$, GW_{72} and Δ_{all}. Different estimations of the 95% confidence intervals: profile log-likelihood (blue), delta method (green) and parametric resampling (red).

Chapter 4

The Return Period of Catalogue Wind Storms

In this chapter we present the main results of this research project, namely the RPs of the storms listed in the PartnerRe wind storm catalogue (referred to as *catalogue storms*, see section 2.1). We start by presenting results from the EWI, then the results from the grid point analysis.

4.1 The extreme wind distribution based on extreme wind indices

Using the EWI defined in section 2.3 we intercompare both the indices and the use of wind gust and geostrophic wind speed in the estimation of the RPs of 96 catalogue storms. Firstly, we introduce the RL/RP plot which forms the main diagram we will use to show the results. The RL/RP plot summarises the fitted GPD (i.e. the extreme value climatology) together with the estimates of the RP and RL of each of the catalogue wind storms (catalogue storms) which are above the chosen threshold. Figure 4.1 is an example of such a plot and shows that using this particular index and domain ($Q95$, GW_{72} and Δ_{land}) we estimate a wide range of RPs (red lines) for the catalogue storms between approximately 0.2 and 100 years. These estimates are based on the GPD fit (black line) and not the cluster maxima (black dots). Notice that some of the cluster maxima (black dots, also known as plotting points) lie slightly outside the 95% confidence intervals, indicating that we may be close to the lowest threshold possible to justify the asymptotic GPD rule. Nonetheless, we chose the 90th percentile as the threshold for all indices, based on a compromise between having a good fit and including as many catalogue storms above the threshold as possible (see section 3.2 for more details).

On the following pages we present the RPs of the catalogue storms for each index and for each of the three domains, all grid points, land only grid points and sea only in figures 4.2 to 4.5. One of the most notably features of all the RL/RP plots is that the GPD fit has a negative shape parameter, ξ, as shown by the negative curvature of the GPD fits (black lines). This implies that the extreme wind distribution, as expressed through the EWI, has a finite upper bound. This is again what we would expect from physical considerations, that there is some limiting value to the highest wind speed possible given energy constraints. Another notable feature is the larger spread of the RPs (and generally higher) of the storms when considering only grid points over land compared with RPs calculated using either the whole domain or grid points over sea only. This is understandable given that the storm catalogue is focused on storms that had a significant impact on various parts of continental Europe and is not focused on storms, possibly more severe, over the north east North Atlantic ocean for example. This is evident for example in figure 4.5 where it is seldom that the RP of a catalogue storm exceed 5 years. There are approximately 40 storms (black dots) that are more severe than any of the storms in the storm catalogue (red lines), in terms of their extreme wind index over the ocean regions of the domain. Considering land points only (figure 4.3) we see that for most EWI, the storm catalogue

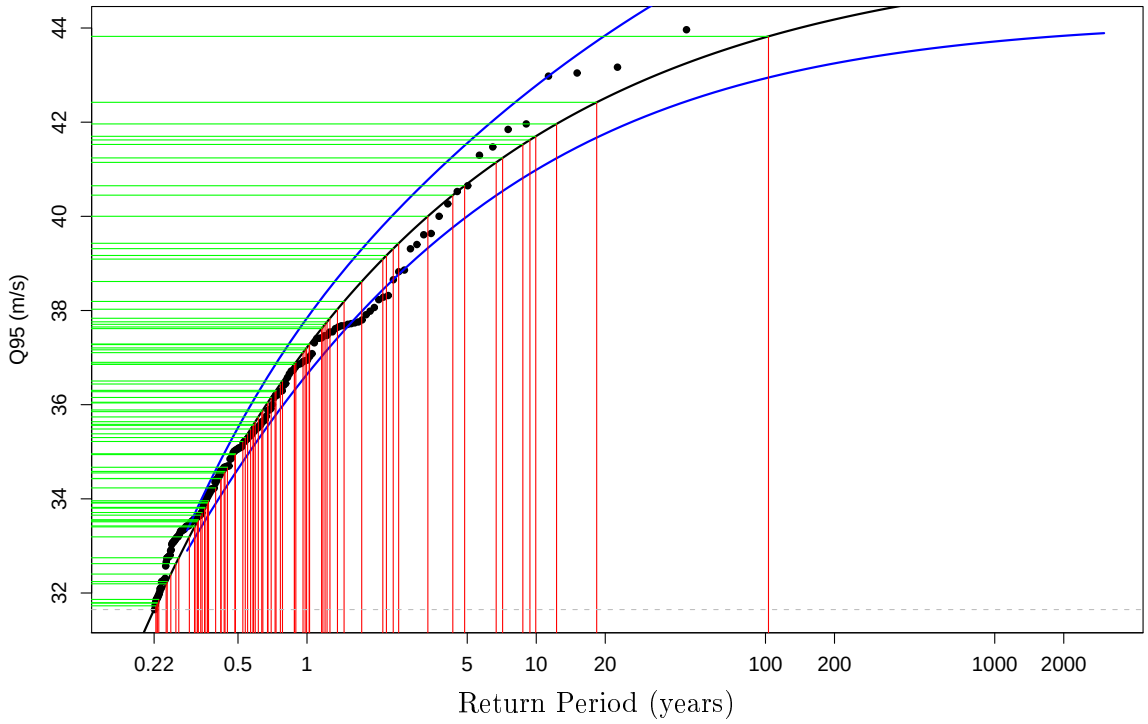

Figure 4.1: The Return Period (RP, years) and Return Level (RL, m/s) of the GPD fit (black line, equation 3.5) of the extreme wind index $Q95$, using geostrophic wind (GW_{72}) over the European land domain (Δ_{land}). The black dots represent the maxima of the declustered POT series. Blue lines show the upper and lower bounds of the 95% confidence interval of both RL and RP calculated using profile log likelihood. The horizontal green and vertical red lines denote the RL and RP of the catalogue storms respectively. The dashed grey line denotes the 90th percentile threshold above which the declustered peaks were chosen. Note the log scale on the horizontal axis.

represents the range of possible RPs well, i.e. the catalogue storms in many cases coincide with the plotting points (the cluster maxima) of the ERA-40 derived EWI. There are storms that appear in the ERA-40 EWI which are not included in the storm catalogue. Notice that the index $SQ95$ performs poorly in terms of capturing the severity of the catalogue storms over all domains. Nonetheless we considered it important to show the results of this index to highlight that some EWI are better than others in capturing the storminess of a region. In some plots it is clear that the GPD fit is not optimal, for example in figure 4.5f) and i) where the 95% confidence interval does not contain the plotting points in the middle section of the GPD fit (1-10 years). This is also evident, for land only areas, in the qq-plots shown in figure 4.4. As explained above, this could be due to choosing a threshold which is not high enough to justify using the GPD or due to the method we used to decluster the data. A comparison between qq-plots for a specific EWI reveals dependence of the GPD fit quality on the declustering method chosen (figure 4.6a and b). Although, practically this has had no major influence on the RP estimates (figure 4.6c).

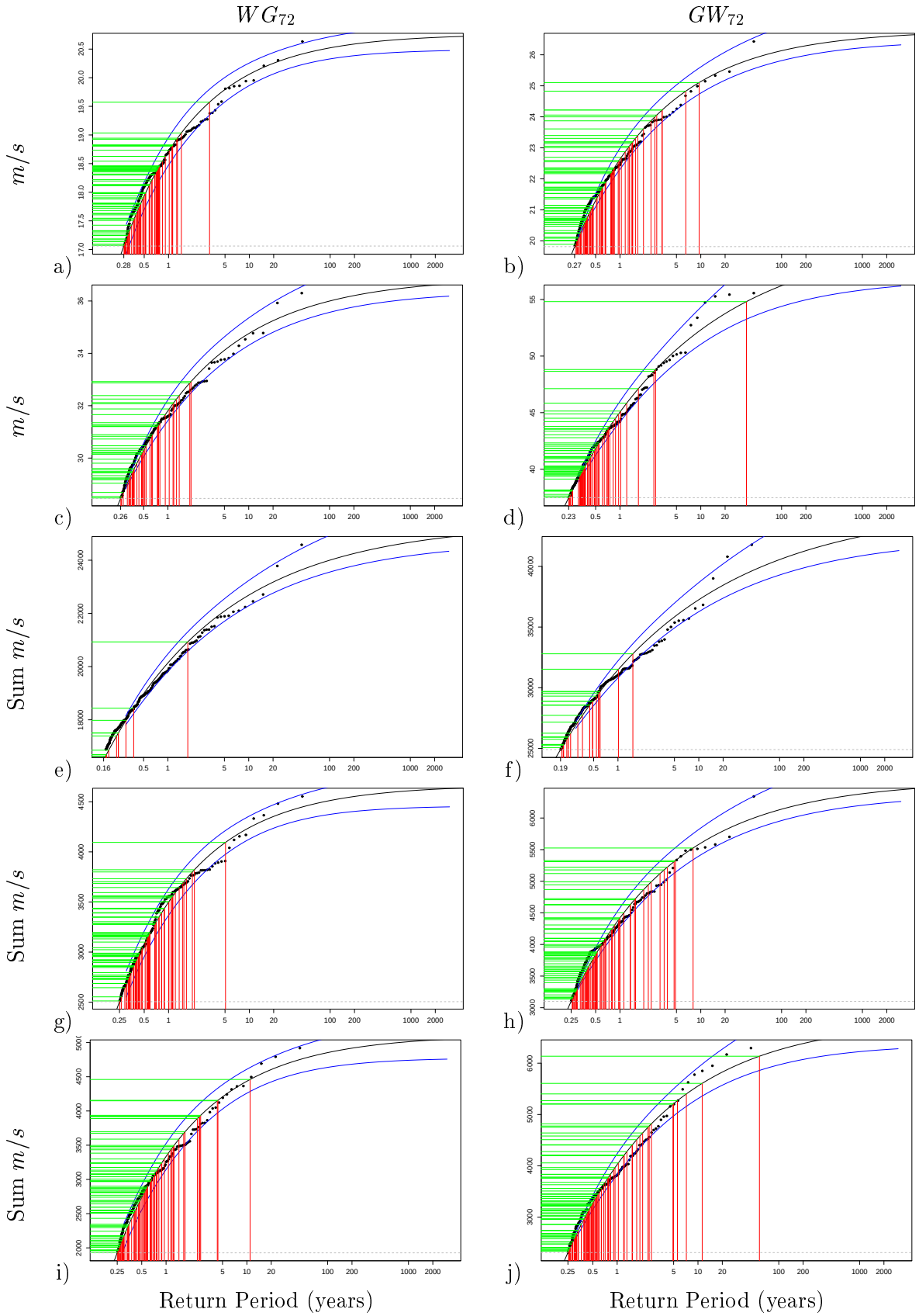

Figure 4.2: The RP and RL of the GPD fit to the five EWIs calculated over the whole domain. RL (m/s, vertical axis) versus RP (years, horizontal axis) with uncertainty (profile log likelihood) estimates. Indices based on WG_{72} and $\Delta_{all-masked}$ (left column) and indices based on GW_{72} and Δ_{all} (right column). a) and b) $\bar{X}$, c) and d) $Q95$, e) and f) $SQ95$, g) and h) $Sfq95$, i) and j) $Sfq95q99$. Green and red lines indicate the RL and RP of the the 96 PartnerRe storms within the ONDJFMA season. The dashed grey line denotes the 90th percentile threshold above which the declustered peaks were chosen.

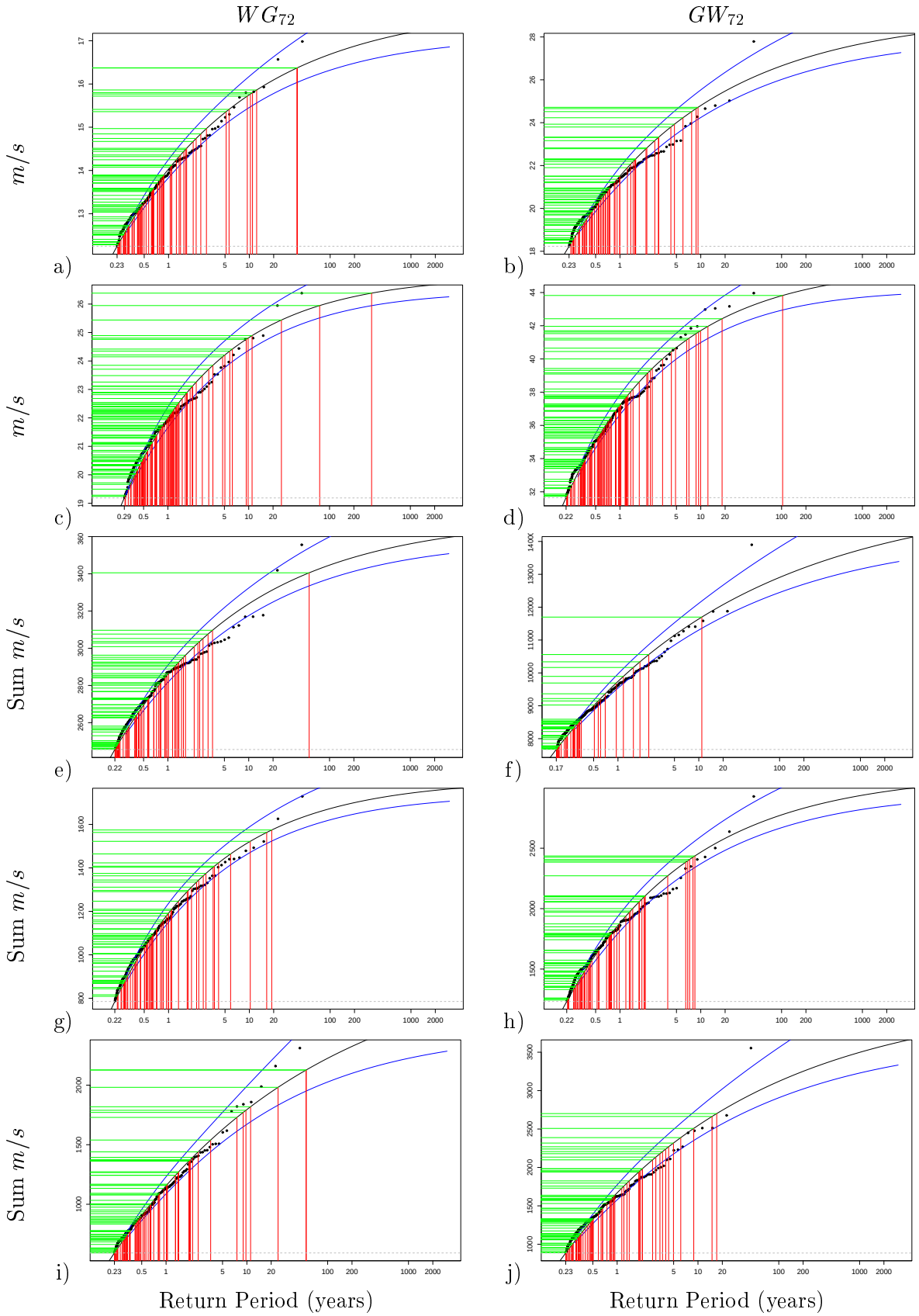

Figure 4.3: The RP and RL of the GPD fit to the five EWIs calculated over land. RL (m/s, vertical axis) versus RP (years, horizontal axis) with uncertainty (profile log likelihood) estimates. Indices based on WG_{72} and $\Delta_{land-masked}$ (left column) and indices based on W^{850}_{72geo} and Δ_{land} (right column). a) and b) $\bar{X}$, c) and d) $Q95$, e) and f) $SQ95$, g) and h) $Sfq95$, i) and j) $Sfq95q99$. Green and red lines indicate the RL and RP of the the 96 PartnerRe storms within the ONDJFMA season. The dashed grey line denotes the 90th percentile threshold above which the declustered peaks were chosen.

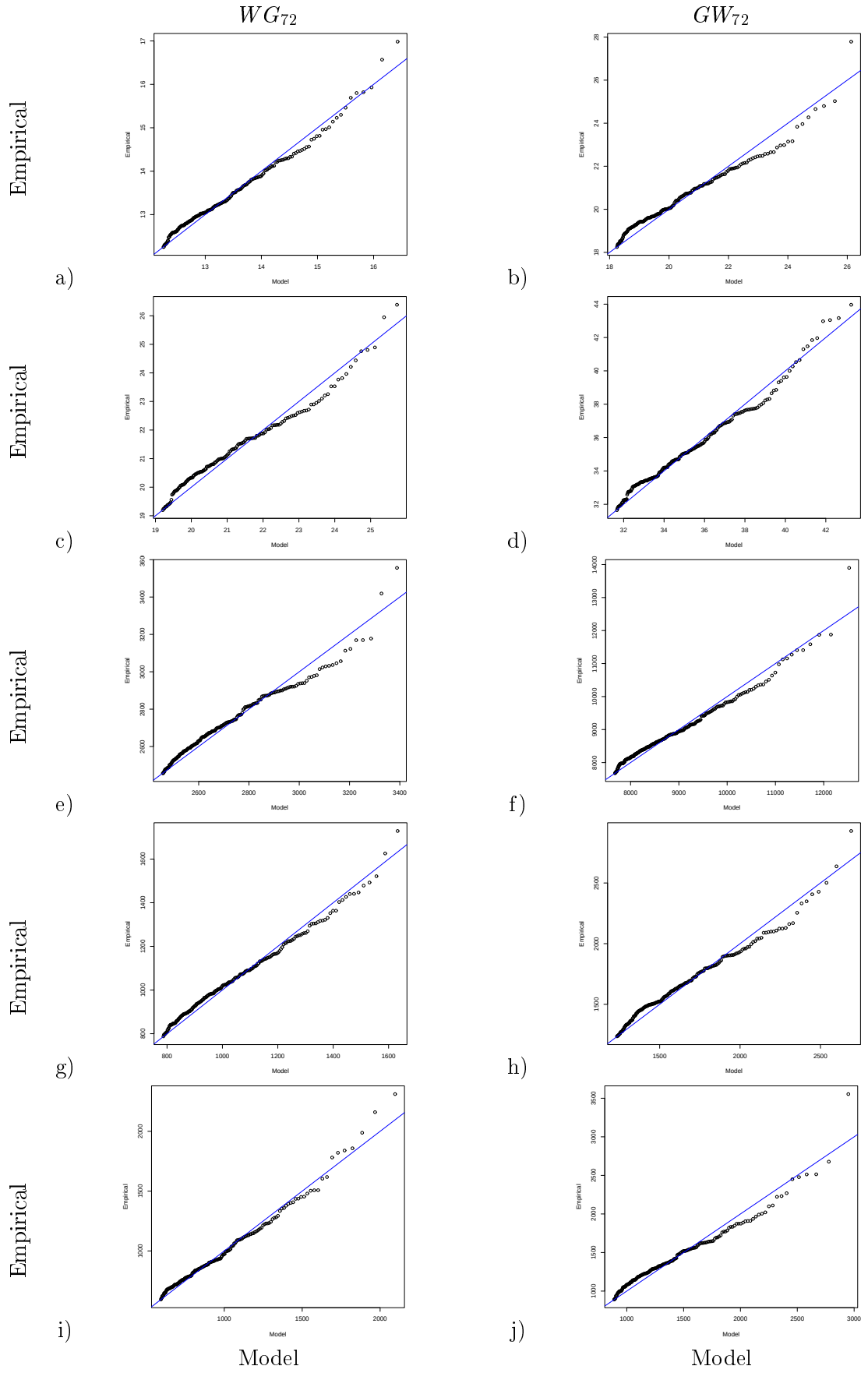

Figure 4.4: Quantile-quantile plots for the GPD fit to the five EWIs calculated over land. Empirical (vertical axis) versus model (horizontal axis). Indices based on WG_{72} and $\Delta_{land-masked}$ (left column) and indices based on GW_{72} and Δ_{land} (right column). a) and b) $\bar{X}$, c) and d) $Q95$, e) and f) $SQ95$, g) and h) $Sfq95$, i) and j) $Sfq95q99$.

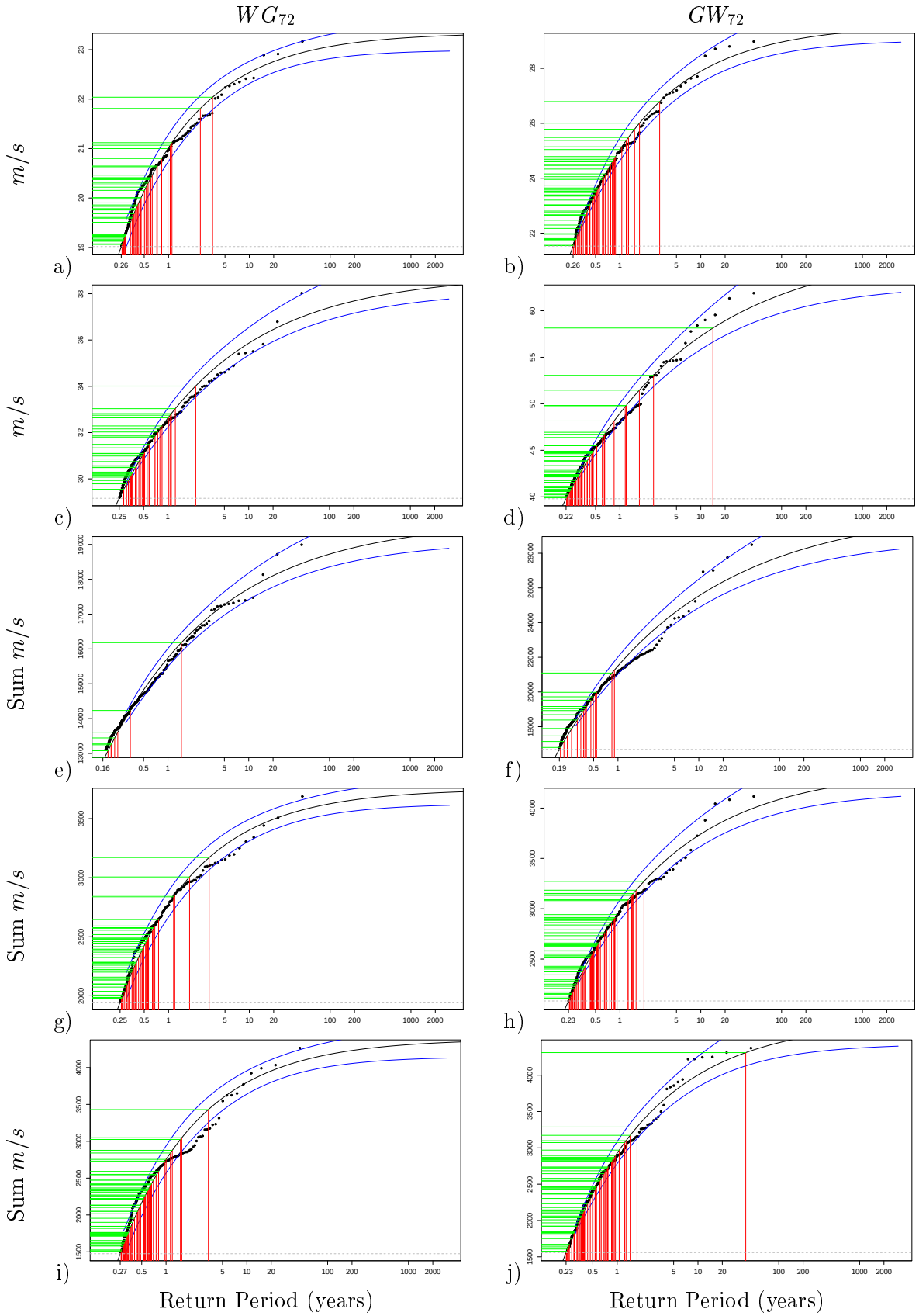

Figure 4.5: The RP and RL of the GPD fit to the five EWIs calculated over sea only. RL (m/s, vertical axis) vs. RP (years, horizontal axis) with uncertainty (profile log likelihood) estimates. Indices based on WG_{72} and $\Delta_{sea-masked}$ (left column) and indices based on GW_{72} and Δ_{sea} (right column). a) and b) $\bar{X}$, c) and d) $Q95$, e) and f) $SQ95$, g) and h) $Sfq95$, i) and j) $Sfq95q99$. Green and red lines indicate the RL and RP of the the 96 PartnerRe storms within the ONDJFMA season. The dashed grey line denotes the 90th percentile threshold above which the declustered peaks were chosen.

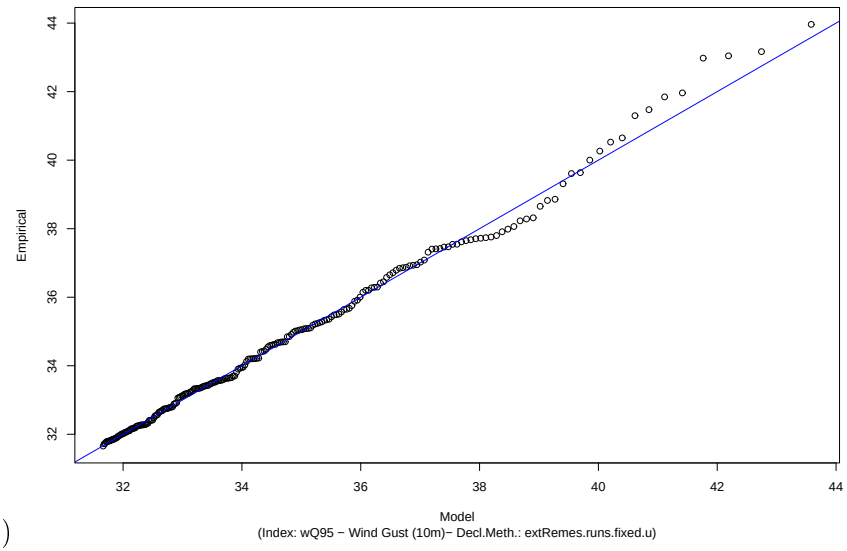

a)

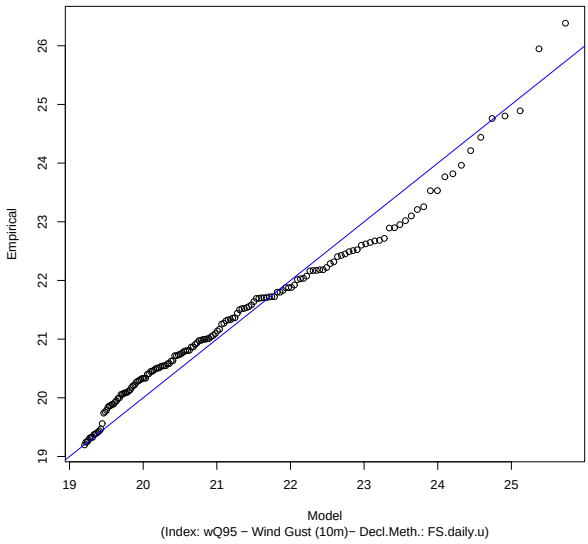

b)

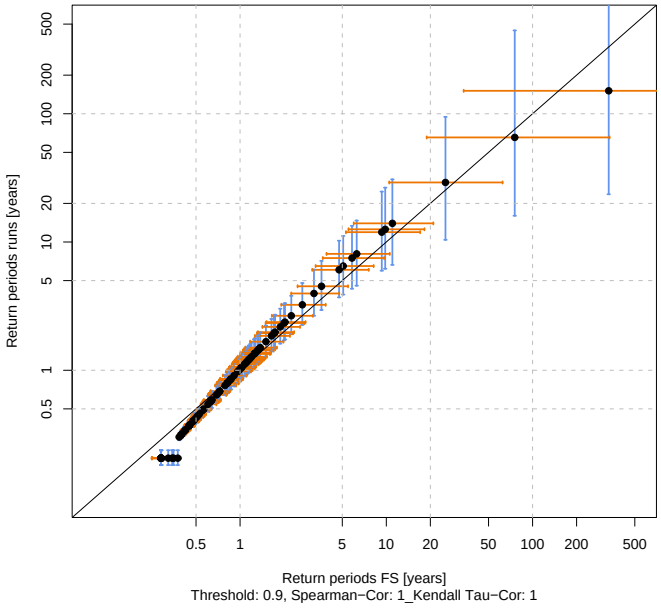

c)

Figure 4.6: Comparison of the fitted GPD using *runs declustering* and the *Ferro and Segers* method. Quantile-quantile plot of $Q95$, WG_{72}, Δ_{land} using runs declustering a) and Ferro and Segers (2003) b). In c) a scatter plot of the RPs of catalogue storms comparing the two methods. Note the logarithmic scale. 95% confidence intervals for each of the RP are denoted by orange (Ferro and Segers, 2003) and blue (runs declustering) whiskers on each scatter plot point. Solid black line denotes the equal RP line. At the bottom of each sub-figure is the Spearman rank and Kendall's Tau correlation coefficient.

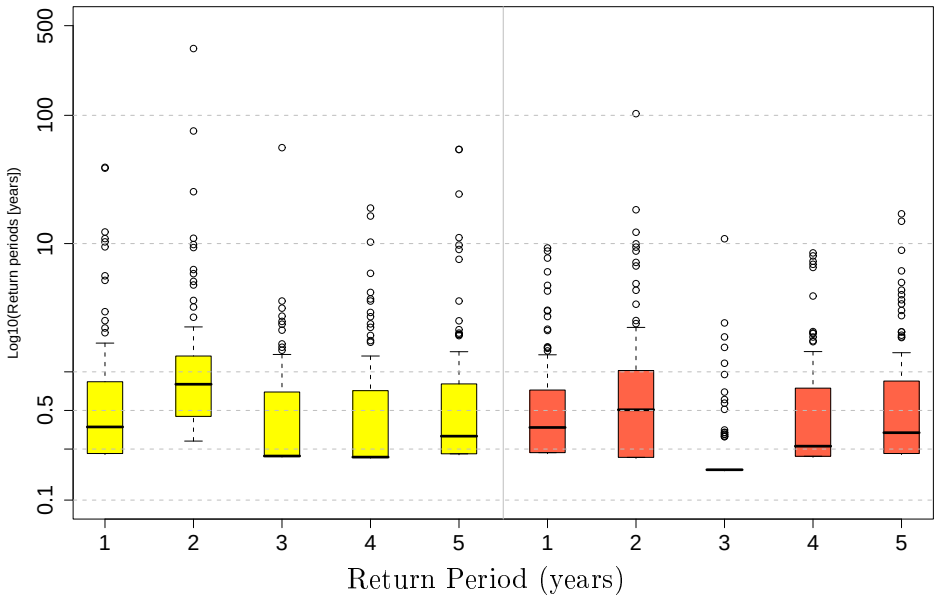

Figure 4.7: A summary of the range of Return Periods (RP, years) of the catalogue storms given by each of the five extreme wind indices (section 2.3) using wind gust (WG_{72} left, yellow boxplots) and geostrophic wind (GW_{72}, right, red boxplots) over the European land domain (Δ_{land} and $\Delta_{land-masked}$ respectively). The numbers on the horizontal axis refer to the EWIs, $\bar{X}$, $Q95$, $SQ95$, $Sfq95$, and $Sfq95q99$, respectively. The solid black line of each boxplot represent the median, the interquartile range (coloured area), 1.5 times the interquartile range (dashed black line) and the outliers (open circles).

Figure 4.7 summarises the range and distribution of return period estimates for each EWI calculated using the two different datasets over land. It is clear that the range and magnitude of RPs for each index except $SQ95$ are similar for each dataset. However, as we will see in the next section the calculated RPs for individual storms varies considerably.

We wished to investigate what effect the use of either WG_{72} or GW_{72} had on the RPs estimated from the derived EWI. Figures 4.8 to 4.12 present scatter plots of the RPs of the PartnerRe storms estimated using WG_{72} versus the RPs using GW_{72} for each index and for each of the domains, all grid points, land only and sea only. On each plot there are 96 points (the number of catalogue storms in the October - April season). For each point the 95% confidence interval for each RP is shown in either red (WG_{72}) or blue (GW_{72}). Generally, there are poor relationships between the RPs of the catalogue storms calculated using the extreme indices and WG_{72} and GW_{72}. In figures 4.8a to 4.12a, ($\Delta_{all-masked}$ and Δ_{all}), we can see that the RPs of the catalogue storms are generally higher when calculated from GW_{72}. When considering land only ($\Delta_{land-masked}$ and Δ_{land}) RP relationships (figures 4.8b to 4.12b) there are generally higher RPs estimated for the storms but also a larger difference in the RP of each storm not explained by the uncertainty of the EVA. For example, in figure 4.9b there is a storm which has a RP estimate of approximately 70 years using $Q95$, WG_{72} whereas the same storm using $Q95$, GW_{72} is only estimated to be 2 year RP event. The relationship between the $SQ95$, again is clearly the worst performing EWI. We discuss the potential causes of these discrepancies later in the report. There is generally a tighter grouping of the RP estimates when sea only grid points are used ($\Delta_{sea-masked}$ and Δ_{sea}, figures 4.8c to 4.12c), however, even though the RPs are lower in many cases the differences in the RPs cannot be explained by the GPD fit uncertainty. In many of the figures it is evident that some storms have the lowest return period possible (approximately 0.3 years or lower). Any storm which was not above the fixed POT threshold was given the same return period of $1/\lambda$ as explained in section 3.3.

a)

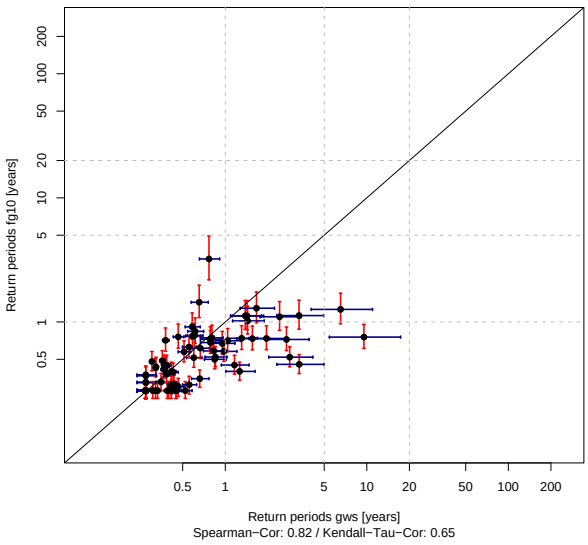

b)

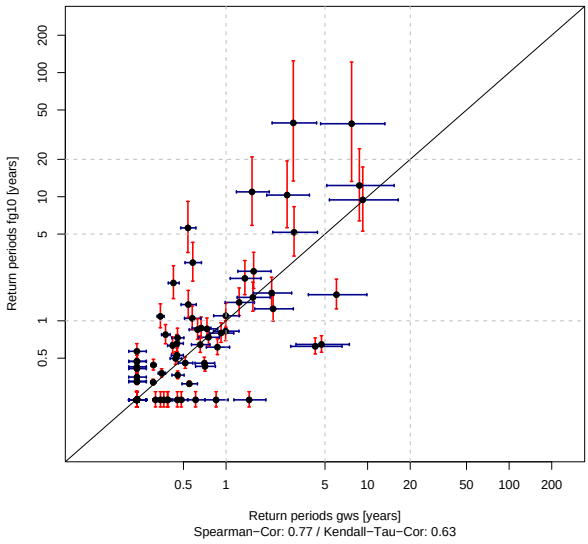

c)

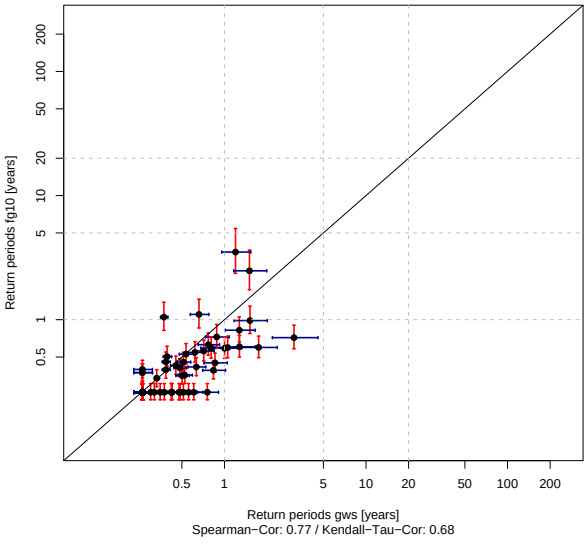

Figure 4.8: Comparison of Return Periods (RP, years) for the 96 PartnerRe wind storms calculated using the extreme wind index (EWI, $\bar{X}$) based on wind gust (WG_{72}, labelled as fg10 on the plot) and geostrophic wind speed (GW_{72}, labelled as gws on the plot). Note the logarithmic scale. 95% confidence intervals for each of the RP are denoted by red (WG_{72}) and blue (GW_{72}) whiskers on each scatter plot point. a) using domain $\Delta_{all-masked}$ and Δ_{all}, b) using domain $\Delta_{land-masked}$ and Δ_{land}, c) using domain $\Delta_{land-masked}$ and Δ_{sea} for WG_{72} and GW_{72} respectively. Solid black line denotes the equal RP line. At the bottom of each sub-figure is the Spearman rank and Kendall Tau correlation coefficient.

a)

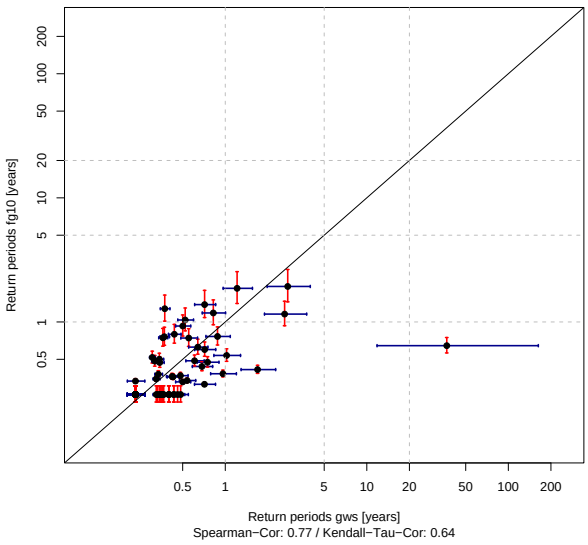

b)

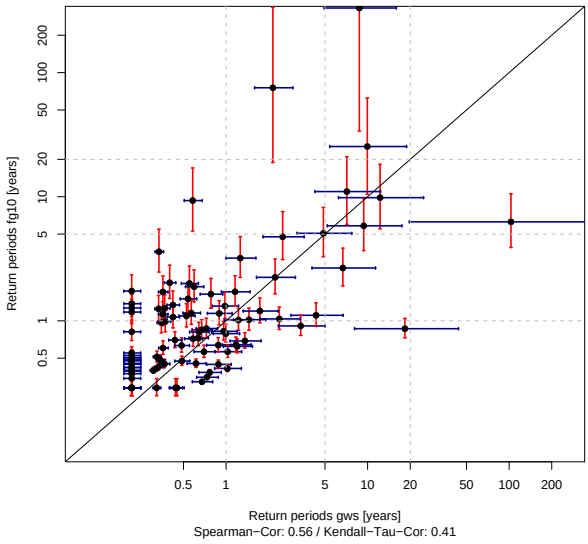

c)

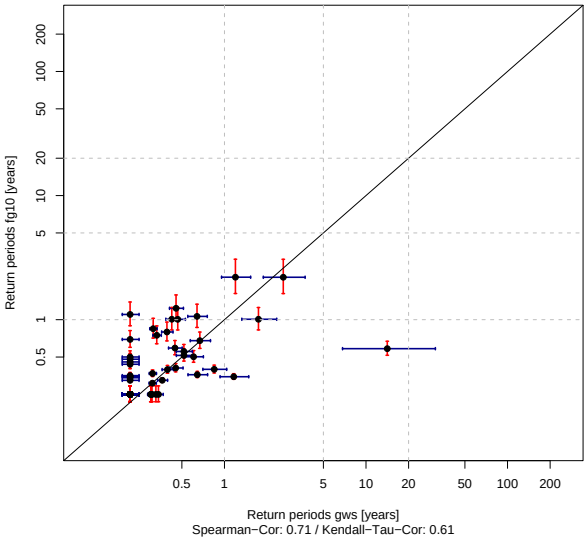

Figure 4.9: As for figure 4.8 but using $Q95$

a)

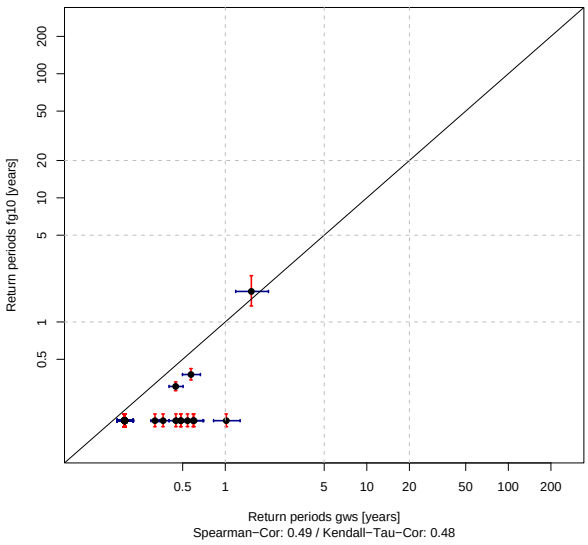

b)

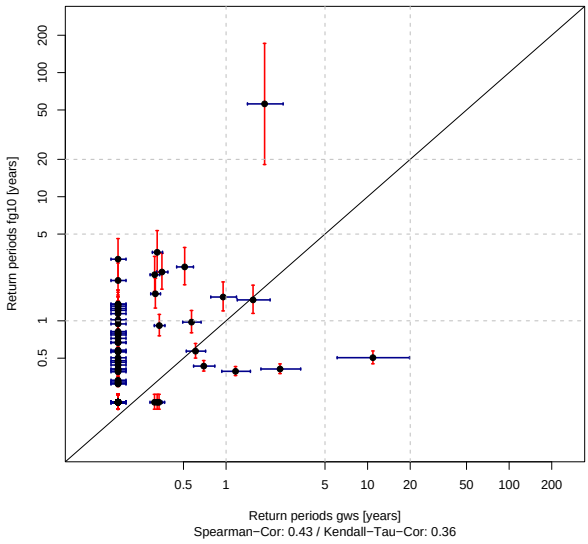

c)

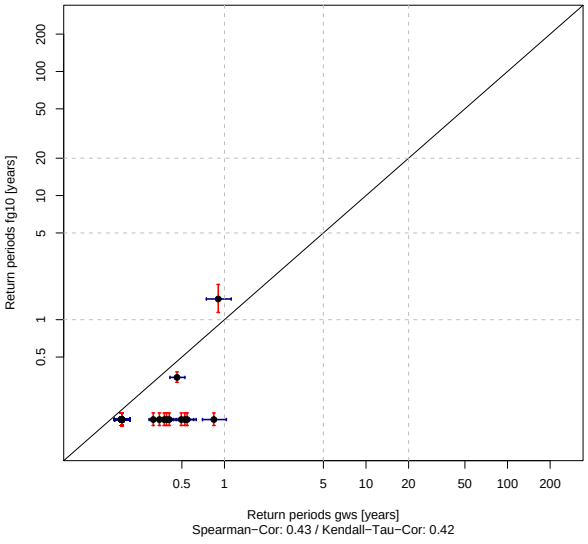

Figure 4.10: As for figure 4.8 but using $SQ95$

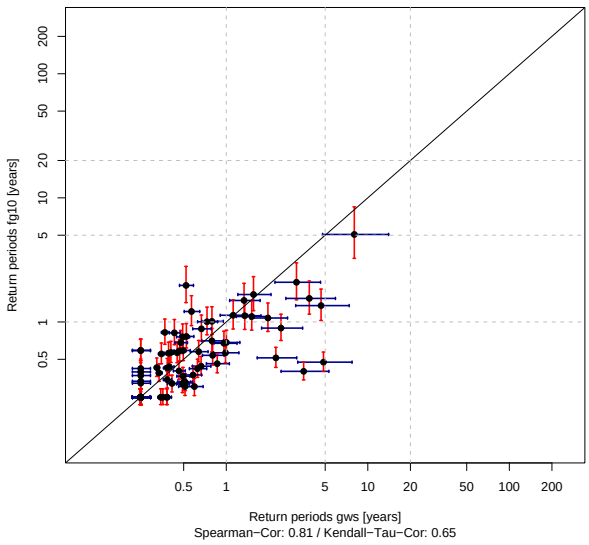

a)

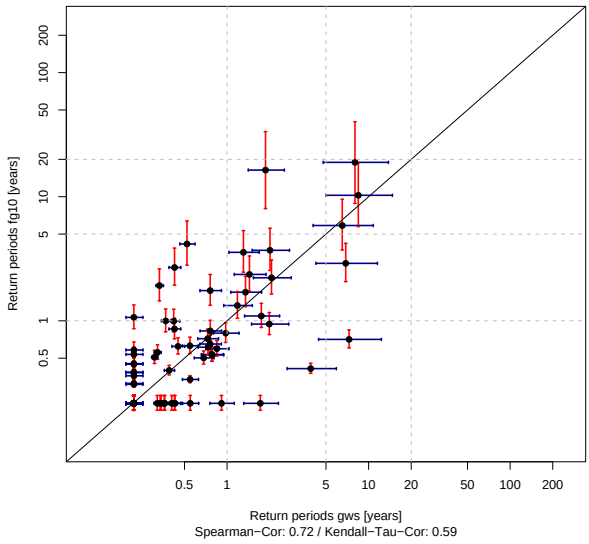

b)

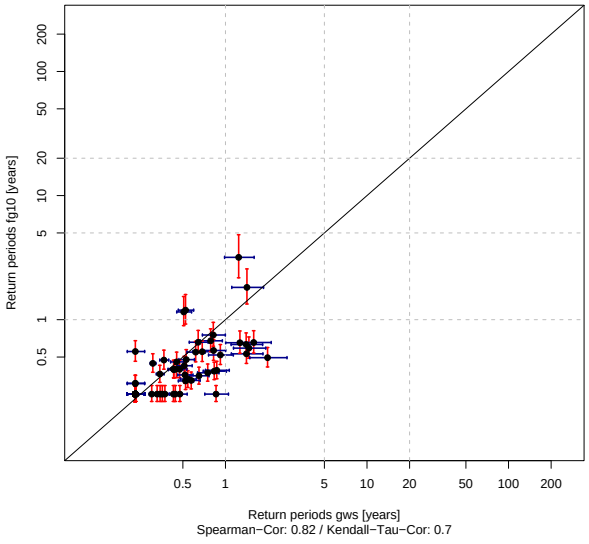

c)

Figure 4.11: As for figure 4.8 but using $Sfq95$

a)

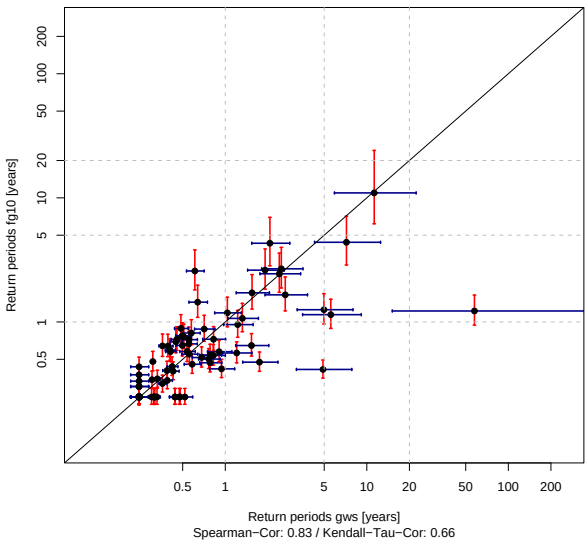

b)

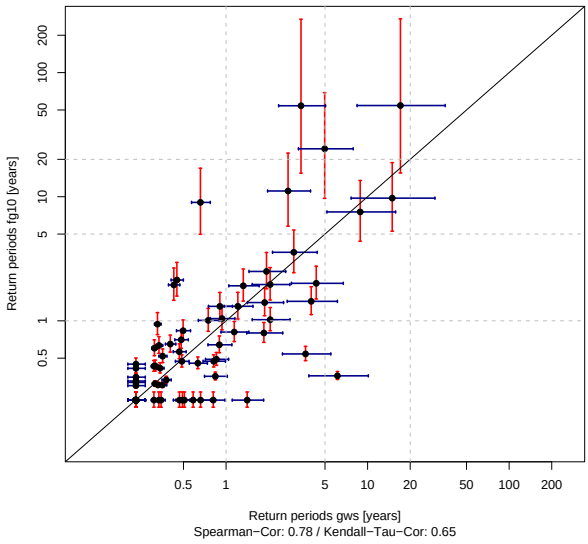

c)

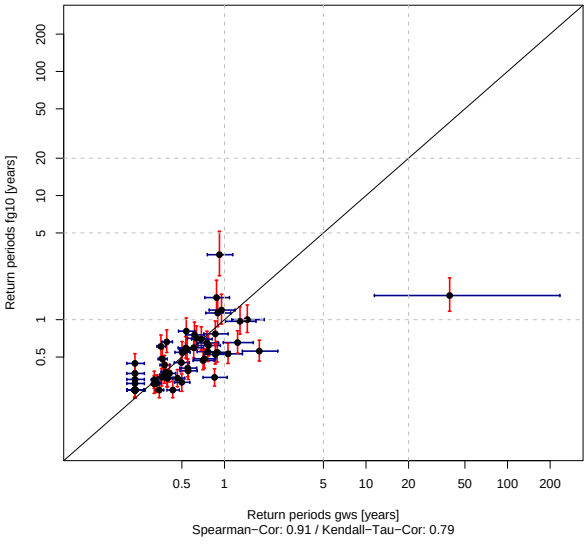

Figure 4.12: As for figure 4.8 but using $Sfq95q99$

We summarise the effects of using different wind data and different EWIs to estimate the RPs of the catalogue storms using the Spearman rank correlation coefficient. In table 4.1 we present the Spearman rank correlation between RPs calculated for each possible combination of EWI, wind data and mask. The results are varied, with some EWI, data and mask combinations resulting in very similar RP estimates, while others are very different from one another. From such an analysis is it hard to extract information on the relative effects that EWI, base data and mask have on the RP estimates, nonetheless we highlight some of the results of this analysis. Inter-index comparisons show that $\bar{X}$, $Sfq95$ and $Sfq95q99$ are the most highly correlated with each other for both data sets (WG_{72} and GW_{72}) and for all masks. Inter-dataset indices which show the highest correlations are $\bar{X}$, $Sfq95$, $Sfq95q99$. Note that the highest inter-index correlations are higher than the highest inter-dataset correlations, indicating that greater differences between RP estimates are due to the dataset rather than the best EWIs shown here. However, if we consider the indices $\bar{X}$ and $Q95$ only we see that the inter-dataset correlations are higher than the inter-index correlations. This highlights the difficulty in trying to establish the main cause for the differences in the RP estimates.

We tried to isolate the effect of using the mask on WG_{72} (land only) by comparing the GW_{72} masked and unmasked RP estimates. Firstly we recall the comparison between the RPs using WG_{72}, $\Delta_{land-masked}$ and GW_{72}, Δ_{land} and we see that the their is a fair relationship between the two data sets (figure 4.13a). If we mask the GW_{72} as if it were WG_{72} with $\Delta_{land-masked}$ and compare the RPs we can see a slight improvement of the Spearman rank correlation from 0.55 to 0.66 (figure 4.13b). However, the main cause for the discrepancies in the RPs is due to the base data set and not the application of the mask as demonstrated by figure 4.13c where we see that the correlation between GW_{72}, $\Delta_{land-masked}$ and GW_{72}, Δ_{land} is much higher (0.86).

ALL

	WG_wMean	WG_wQ95	WG_S_gr_wQ95	WG_wSf_q95	WG_wSf_q95_99	GW_wMean	GW_wQ95	GW_S_gr_wQ95	GW_wSf_q95	GW_wSf_q95_99
WG_wMean	1									
WG_wQ95	0.63	1								
WG_S_gr_wQ95	0.018	0.307	1							
WG_wSf_q95	0.914	0.519	-0.096	1						
WG_wSf_q95_99	0.879	0.699	0.071	0.894	1					
GW_wMean	0.823	0.453	-0.075	0.823	0.763	1				
GW_wQ95	0.701	0.772	0.132	0.586	0.705	0.637	1			
GW_S_gr_wQ95	0.253	0.605	0.488	0.155	0.311	0.071	0.447	1		
GW_wSf_q95	0.728	0.398	-0.095	0.807	0.742	0.933	0.526	-0.004	1	
GW_wSf_q95_99	0.727	0.543	-0.001	0.762	0.83	0.865	0.703	0.188	0.883	1

LAND

	WG_wMean	WG_wQ95	WG_S_gr_wQ95	WG_wSf_q95	WG_wSf_q95_99	GW_wMean	GW_wQ95	GW_S_gr_wQ95	GW_wSf_q95	GW_wSf_q95_99
WG_wMean	1									
WG_wQ95	0.591	1								
WG_S_gr_wQ95	0.391	0.715	1							
WG_wSf_q95	0.936	0.523	0.382	1						
WG_wSf_q95_99	0.95	0.583	0.438	0.953	1					
GW_wMean	0.765	0.461	0.215	0.731	0.733	1				
GW_wQ95	0.628	0.557	0.23	0.586	0.628	0.687	1			
GW_S_gr_wQ95	-0.007	0.214	0.429	0.027	0.037	-0.059	0.126	1		
GW_wSf_q95	0.739	0.459	0.243	0.72	0.72	0.962	0.65	-0.034	1	
GW_wSf_q95_99	0.763	0.487	0.317	0.752	0.775	0.909	0.737	0.063	0.915	1

SEA

	WG_wMean	WG_wQ95	WG_S_gr_wQ95	WG_wSf_q95	WG_wSf_q95_99	GW_wMean	GW_wQ95	GW_S_gr_wQ95	GW_wSf_q95	GW_wSf_q95_99
WG_wMean	1									
WG_wQ95	0.563	1								
WG_S_gr_wQ95	0.144	0.256	1							
WG_wSf_q95	0.873	0.556	-0.014	1						
WG_wSf_q95_99	0.8	0.764	0.174	0.853	1					
GW_wMean	0.773	0.496	-0.008	0.787	0.749	1				
GW_wQ95	0.638	0.709	0.045	0.63	0.714	0.664	1			
GW_S_gr_wQ95	0.321	0.597	0.429	0.267	0.445	0.205	0.352	1		
GW_wSf_q95	0.754	0.528	0.011	0.822	0.782	0.934	0.606	0.219	1	
GW_wSf_q95_99	0.704	0.694	0.124	0.762	0.908	0.834	0.745	0.348	0.865	1

Table 4.1: The Spearman rank correlation between the Return Periods (RP) of catalogue storms (96 storms) calculated from different extreme wind indices (EWI, yellow shaded boxes, also described as *inter-index*) and different datasets (either WG_{72}or GW_{72}, red shaded boxes, also described as *inter-dataset*) over all grid points a), land only grid points b) and sea only grid points c). The labels "WG" and "GW" refer to wind gust and geostrophic wind respectively. The labelling of the EWIs is different to that in the text, however the order of the indices is the same as the order given in section 2.3.

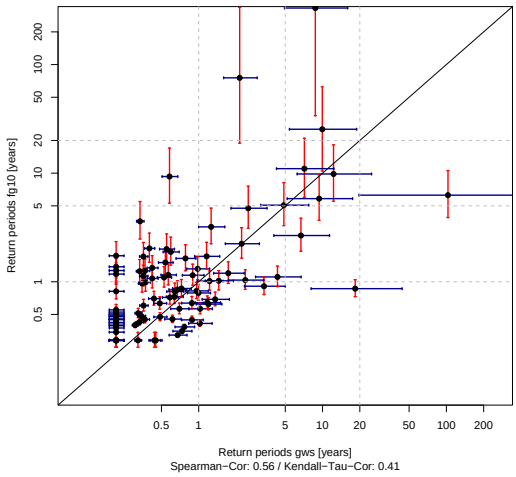

a)

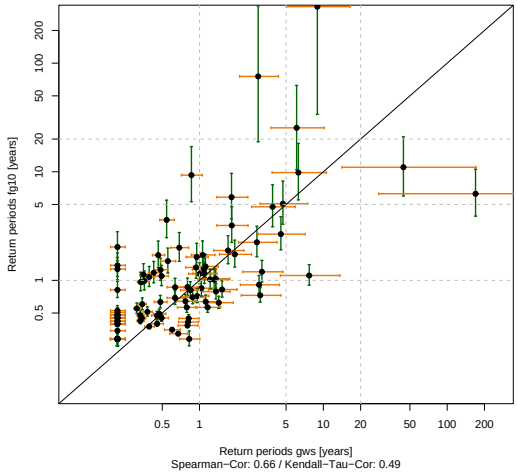

b)

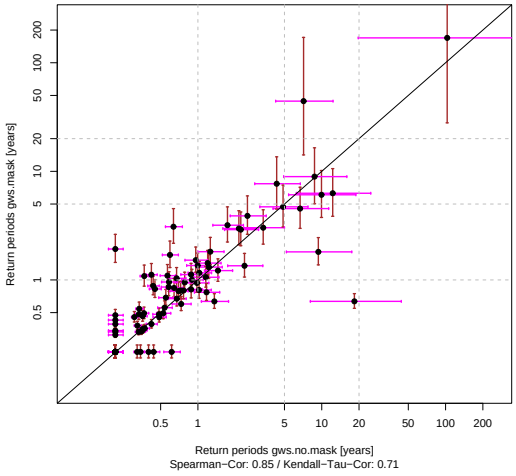

c)

Figure 4.13: The effect of masking unrealistic wind gust grid points on return period estimates. Scatter plot of RPs (years) for the 96 catalogue wind storms calculated using $Q95$, WG_{72} versus the RPs calculated using $Q95$, GW_{72}. a) using domain $\Delta_{land-masked}$ and Δ_{land}, b) using domain $\Delta_{land-masked}$ and $\Delta_{land-masked}$ for WG_{72} and GW_{72} respectively and c) using GW_{72} domain $\Delta_{land-masked}$ and Δ_{land}. Solid black line denotes the equal RP line. Note the logarithmic scale. 95% confidence intervals for each of the RP are denoted by red and blue (green and orange) for $WG_{72}$and GW_{72} in a) and b) and in c) the colours brown and purple are used to denote the RP confidence intervals of GW_{72} $\Delta_{land-masked}$ and Δ_{land} respectively. At the bottom of each sub-figure is the Spearman rank and Kendall Tau correlation coefficient.

4.2 The extreme wind distribution at each grid point

We fitted a GPD distribution to each of the 10857 grid points over the domain to form an extreme wind climatology which is more representative of the local extreme wind climatology than the extreme wind index approach. As described in section 3.2 we used a higher fixed threshold (95% quantile) in the GPD model than with the EWI (90% quantile) based on the extensive diagnostic checks performed for individual grid points. The EVA for each grid point is exactly the same as that for the EWI except that we use the raw 6 hourly data and not the 72 hour maximum. An example of typical GPD fits to individual grid points together with their quantile plots are shown in figure 4.14. In these examples some of the cluster maxima lie outside of the confidence intervals, however this was found to occur in only a small proportion of the grid points .

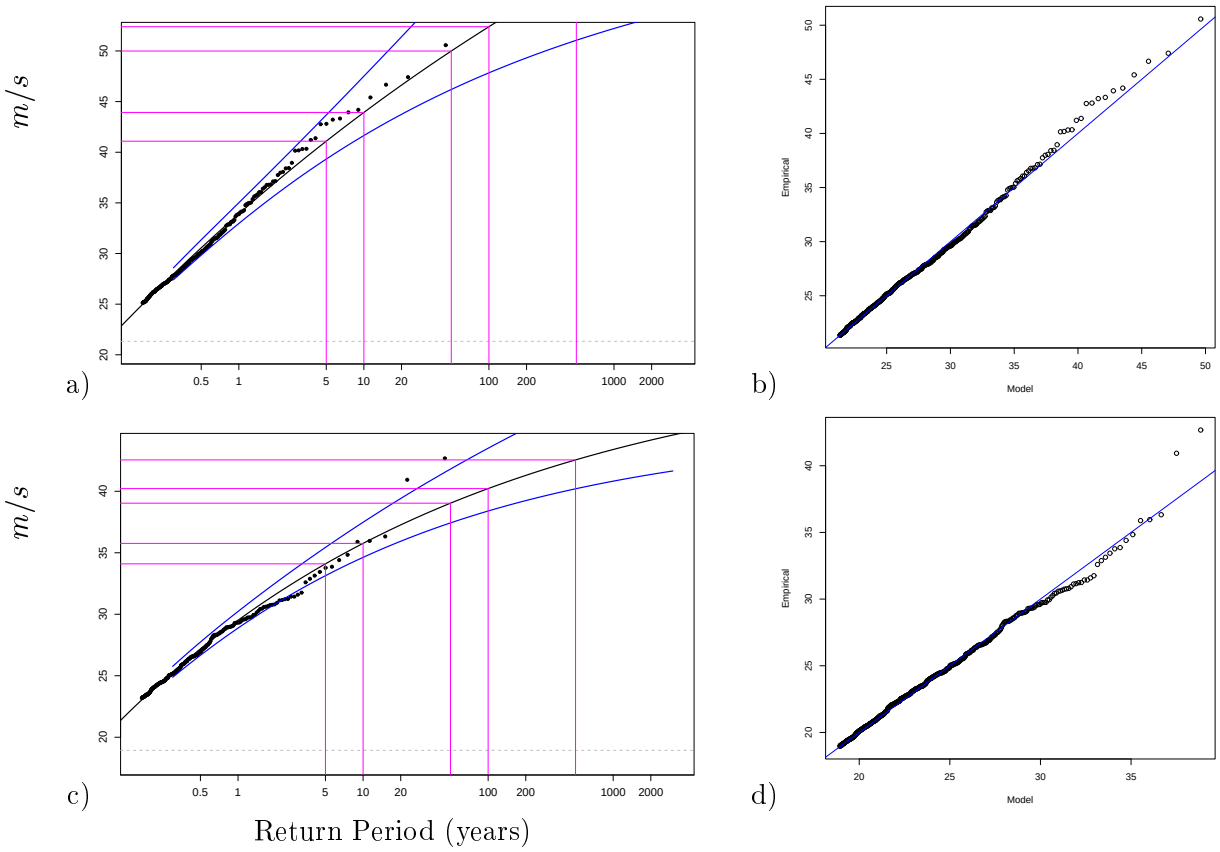

Figure 4.14: The RL (m/s) and RP (years) of the GPD fit to the GW at two grid points in the analysis domain, 2.5° E, 57° N a) and c) 30° W, 67° N. The corresponding quantile-quantile plots are shown in b) and d) respectively.

Figure 4.15 provides a summary of the important parameters of the EVA at each grid point. Figure 4.15a shows the empirically based seasonal 95% quantile threshold used in the extreme wind climatology of ERA-40 using GW. Generally there are higher winds over the North Atlantic Ocean and the British Isle's than over the north, east and south of the domain. The average number of extreme wind events per season, λ shows a band of lower values running from the south west of the domain to the north east of the domain, whereas in the north west and the south east as well as the far north east there are higher values of λ (figure 4.15b). The spatial distribution of σ, the scale parameter of the GPD (equation 3.1), closely resembles the distribution of the u with more variability, i.e. a wider GPD distribution over ocean areas compared to land areas (see Monahan, 2004, for a physical explanation). The shape parameter ξ is rather mixed and shows little spatial coherency except for a tendency for values over land to be more negative than over ocean or sea regions. In some cases individual grid points have a slightly positive shape

parameter indicating that the GPD has no upper limit. The extremal index θ (equation 3.8), a measure of the tendency for storms to cluster in time is almost identical in appearance to the parameter λ shows a wide area of the domain east of the main North Atlantic storm track where θ is lower than around 0.2 (green and yellow colours) indicating that extreme wind events tend to form larger clusters that are separated by more time in this region compared to the western North Atlantic and south of the Alps and the eastern Mediterranean, in part confirming the analysis of Mailier et al. (2006) for cyclone count based statistics. This process is evident in figure 3.5 which shows the declustered POT series for two points, where the are clearly more clusters in latter (figure 3.5a, higher λ and θ) than in the former (figure 3.5b, lower λ and θ).

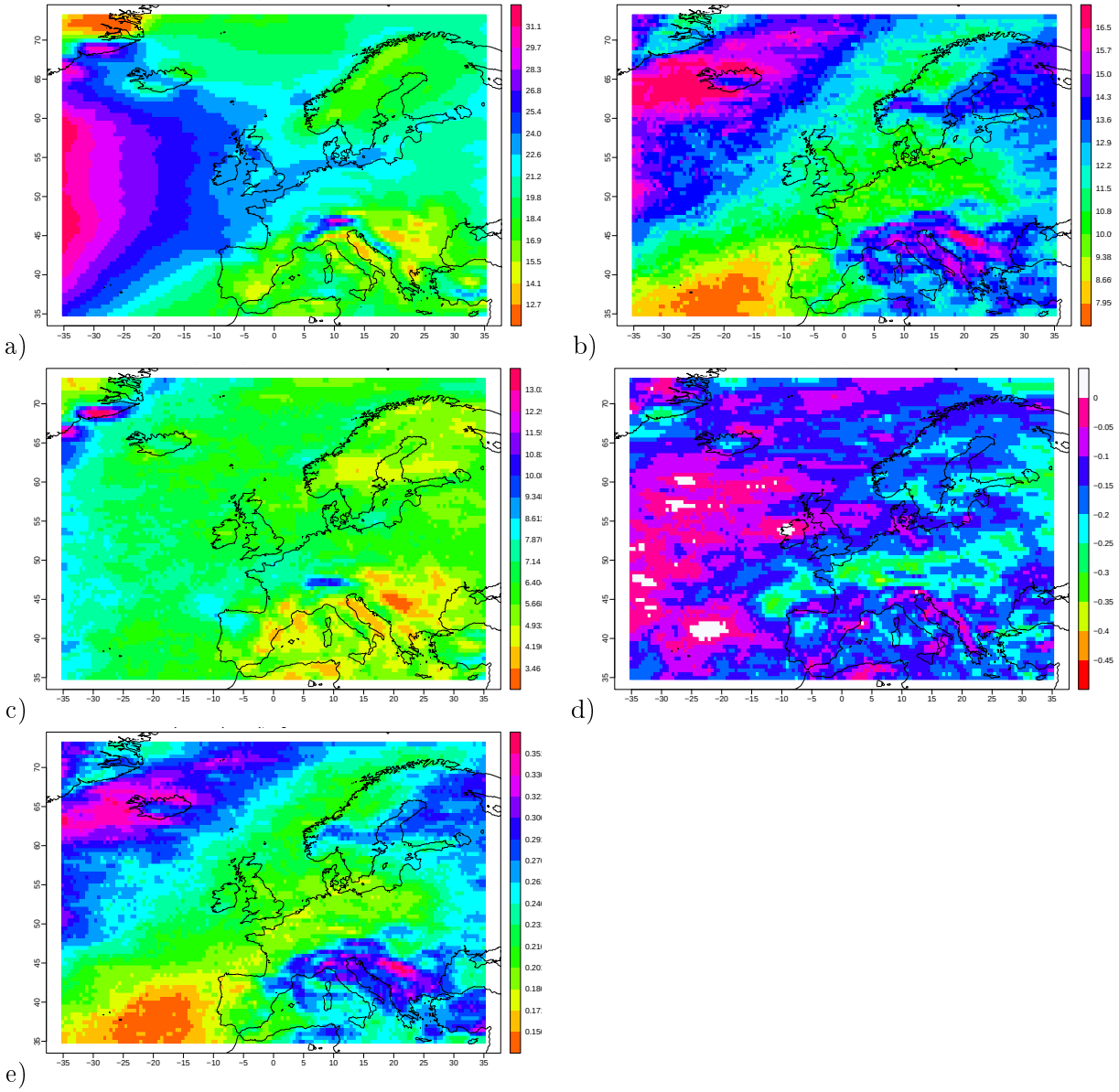

Figure 4.15: Important parameters of the grid point EVA (section 3) based on *GW*. The grid point empirical 95% quantile threshold, u (m/s) a), the MLEs of the GPD fit (equations 3.1 and 3.5) for λ (the average number of declustered exceedances of the 95% quantile threshold) b), σ (the scale parameter of the GPD) c), ξ (the shape parameter of the GPD) d), and the extremal index, θ (equation 3.8) e).

The RL for various RPs are shown in figure 4.16. For each of the RPs a similar spatial structure of the extreme winds can be seen, with higher values in the far west of the domain and over ocean regions than over land. Relatively high values can be seen over British Isle's and the north coast of Spain as well as the western and northern coasts of western Europe with relatively lower values over Scandinavia and eastern and southern Europe.

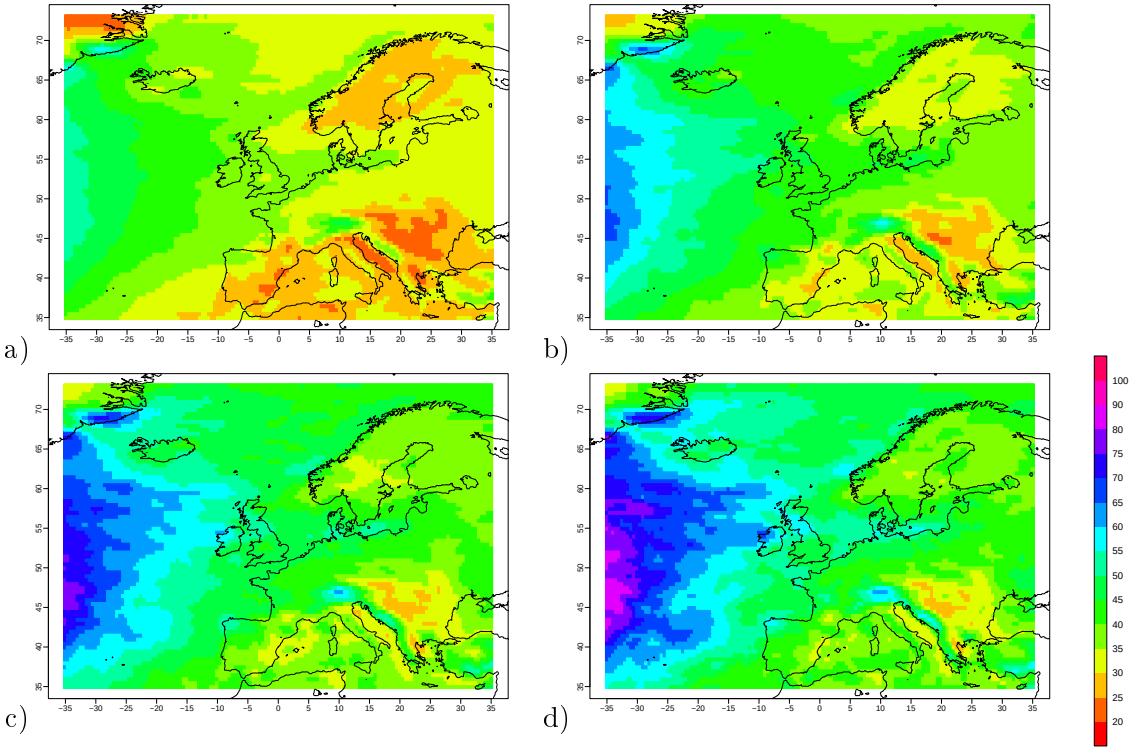

Figure 4.16: The RL of GW at each grid point (m/s) over the extended winter season (October - April), for RPs of 1 year a), 5 years b), 20 years c) and 50 years d).

As for the EWIs, we investigated the effect of using different data to estimate the RP of the catalogue storms at the grid point level. Below we present some selected examples of the RPs calculated using GW or WG. Naturally, we could only compare grid point RPs where both datasets had data which were not masked. It is clear from figure 4.17 that achieving a consistent estimate of RP for each of the catalogue storms at individual grid points is as difficult as when using EWIs and different datasets. In figure 4.17a it is clear that some storms at the location 3° W, 48° N have a very different RP from one another depending on the dataset chosen, while there is better agreement at 5° W, 53° N, especially for storms with higher RPs (4.17b) whereas at 25° E, 55° N (figure 4.17c) shows that the area is less affected by the storms in the storm catalogue. A possible reason for the lack of correspondence between these estimates is demonstrated in figures 4.18 and 4.19. Qualitatively the RP spatial pattern based on WG (figure 4.18a) and GW (figure 4.18b) are the same for the storm Anatol, however, notice that the RPs at the beginning and the end of west-east high RP area are substantially different. We see that the differences between the two grid point analyses are very different for the storm Herta. An aliasing effect using GW (figure 4.19b) is clearly responsible for the differences in the RP patterns.

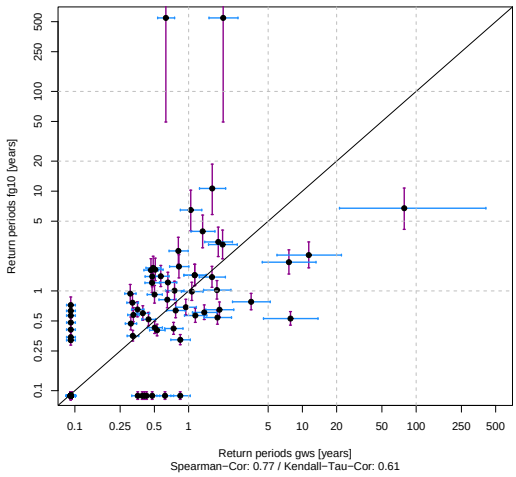

a)

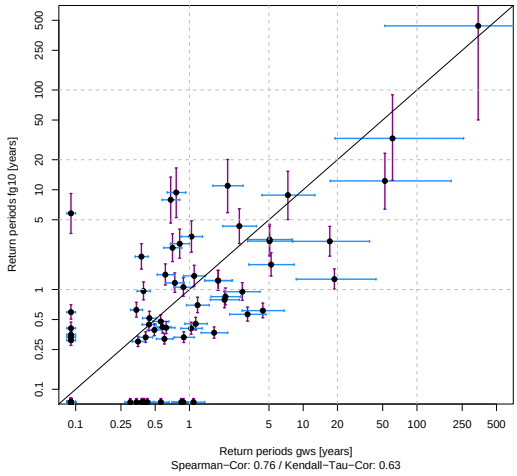

b)

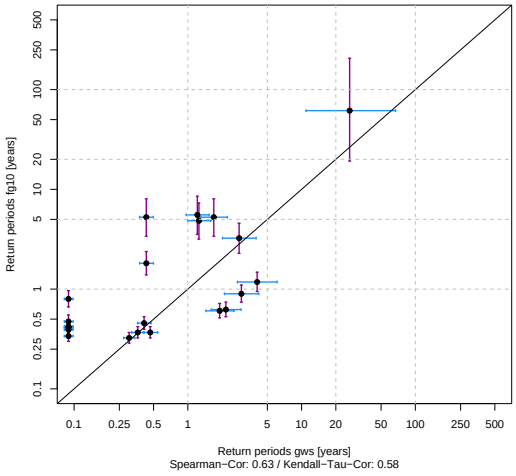

c)

Figure 4.17: Scatter plot of RPs (years) for the 96 catalogue wind storms calculated using WG (labelled fg10 on the plot)versus the RPs calculated using, GW (labelled gws on the plot) at various grid points, a) 3° W, 48° N, b) 5° W, 53° N and c) 25° E, 55° N. Note the logarithmic scale. 95% confidence intervals for each of the RP are denoted by purple (WG) and light blue (GW) whiskers on each scatter plot point. Solid black line denotes the equal RP line. At the bottom of each sub-figure is the Spearman rank and Kendall Tau correlation coefficient.

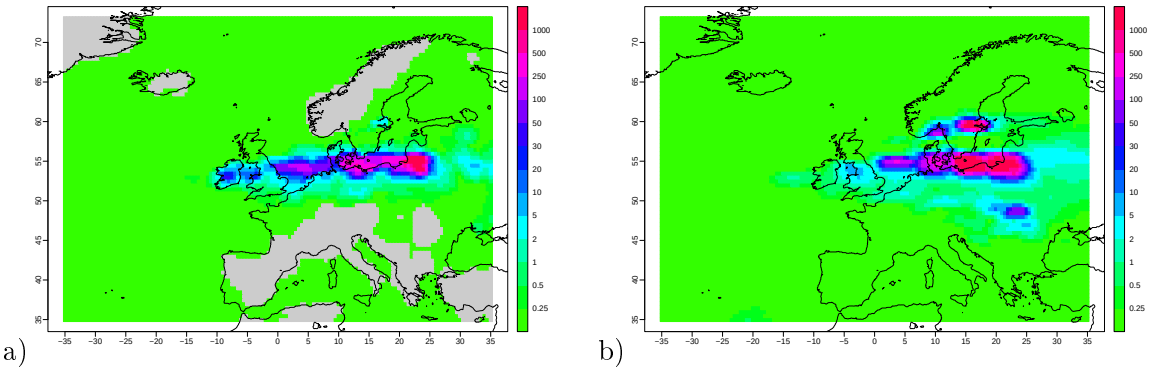

Figure 4.18: The RP (years) for each grid point estimated from a) WG and b) GW for the storm Anatol: 19891215 0600UTC.

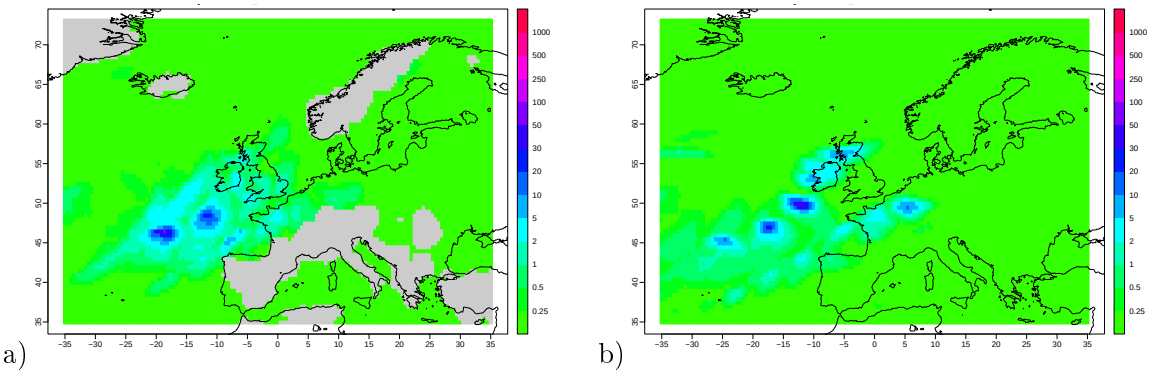

Figure 4.19: The RP (years) for each grid point estimated from a) WG and b) GW for the storm Herta: 19900201 0000UTC.

4.3 The return period of some prominent European wind storms

In this section we present a qualitative comparison of RPs calculated from the EWIs and the grid point approach to demonstrate their utility in estimating the RPs of catalogue storms during the 1989/90 and 1999/2000 extended winter seasons. Tables 4.2 and 4.3 summarise the RPs calculated using the $Q95$ using GW_{72} or WG_{72} over land (Δ_{land}) and the range of grid point RPs over land, using GW or WG respectively. The most severe wind storm in the storm catalogue (according to this index, table 4.2) is associated with the cyclone Daria with a RP estimated to be 103 years, however, the uncertainty associated with this figure is very high. In the grid point analysis the same storm has produced local winds over land to be between 0.25 and 1000+ years with some of the individual grid point RP upper bound of uncertainties as high as 10 000+ years. Qualitatively then, one could say that the EWI and the grid point analysis are in agreement for this storm. However, when we compare the estimates for Herta, Wiebke, Anatol, Lothar, Martin and Kerstin the differences between the local estimates of wind RP and EWI RP estimates are larger, with the RPs based on the EWI much lower than the range of grid point RPs. If we compare RP estimates using the two different datasets then we see large differences. When we use WG_{72} we can see an immediate effect of the masking on the storms Lothar and Martin, whose RP estimates are much lower using WG_{72}, although in section 4.1 we demonstrated that on average, the effect of the mask is minimal. Another major difference visible in the two tables is that the most intense storm estimate using GW_{72} is Daria, whereas this storm only has a RP of around 6 years calculated from WG_{72}. The most severe storm using WG_{72} is Vivian with a RP of 331 years. While the grid point RP analysis also exhibits dependence on the dataset at the grid point level, qualitatively the pattern and magnitude of the RPs as similar (see figure 4.18). The storm Lothar has been studied in detail and our RP estimates are in agreement with

the work of Albisser et al. (2001) and Sacré (2002), who show a range of RPs similar to those estimated from both the EWIs and our grid point analysis.

Storm name	date/time Catalogue storms	lower 0.025 (years)	Return Period (years)	upper 0.975 (years)	grid point return period range (years) over land
unknown	1989-12-15 06:00:00	0.5	0.6	0.7	0.25-1000
Daria	1990-01-23 12:00:00	19.7	103	1840	0.25-1000+
Herta	1990-02-01 00:00:00	0.5	0.6	0.8	0.25-20
Nana	1990-02-10 18:00:00	0.3	0.3	0.4	0.25-5
Vivian	1990-02-24 12:00:00	4.9	8.7	15.9	0.25-500
Wiebke	1990-02-26 06:00:00	5.4	10.0	18.8	0.25-1000+
Anatol	1999-12-01 12:00:00	4.2	7.1	12.3	0.25-1000+
Lothar	1999-12-23 18:00:00	5.2	9.4	17.5	0.25-1000+
Martin	1999-12-25 12:00:00	8	18.3	43.9	0.25-1000+
Kerstin	2000-01-27 00:00:00	0.3	0.4	0.4	0.25-250

Table 4.2: The RPs of some prominent wind storms in the storm catalogue during the 1989/90 and 1999/2000 extended winter season estimated using $Q95$, GW_{72} and Δ_{land}. The last column is an estimate of the range of RPs calculated over land only from the corresponding grid point analyses shown in figures 4.21 & 4.22. The columns denoted *lower* and *upper* refer to the 95% confidence interval boundaries respectively. Note that the date/time field refers to the start date of the 72 hour integration period of the high resolution model runs, see section 2.1 for more details.

Storm name	date/time	lower 0.025 (years)	Return Period (years)	upper 0.975 (years)	grid point return period range (years) over land
unknown	1989-12-15 06:00:00	0.4	0.4	0.5	0.25-5
Daria	1990-01-23 12:00:00	3.9	6.2	10.5	0.25-1000+
Herta	1990-02-01 00:00:00	0.7	0.8	1.0	0.25-5
Nana	1990-02-10 18:00:00	0.5	0.6	0.7	0.25-20
Vivian	1990-02-24 12:00:00	34	331	12351	0.25-1000+
Wiebke	1990-02-26 06:00:00	10.4	25.3	62.3	0.25-1000+
Anatol	1999-12-01 12:00:00	5.9	11.0	21.0	0.25-1000+
Lothar	1999-12-23 18:00:00	3.7	5.8	9.6	0.25-1000+
Martin	1999-12-25 12:00:00	0.7	0.9	1.0	0.25-1000+
Kerstin	2000-01-27 00:00:00	0.9	1.1	1.4	0.25-250

Table 4.3: As for table 4.2 but using the index $Q95$, WG_{72} and Δ_{land}. Plots of grid point RPs are not shown.

As with the EWIs, we also calculated confidence intervals for the return periods of each catalogue storm for each grid point. Figure 4.20 shows the 95% confidence interval for the RPs of grid point wind from the storm Daria. The upper plot (figure 4.20a)) denotes the upper bound of the confidence interval, the middle plot is the best estimate of RP and the lower plot (figure 4.20c) indicates the lower bound of the confidence interval. In the English channel area, where the storm had its highest intensity, the RPs confidence intervals are between approximately 100 years to 1000+ years.

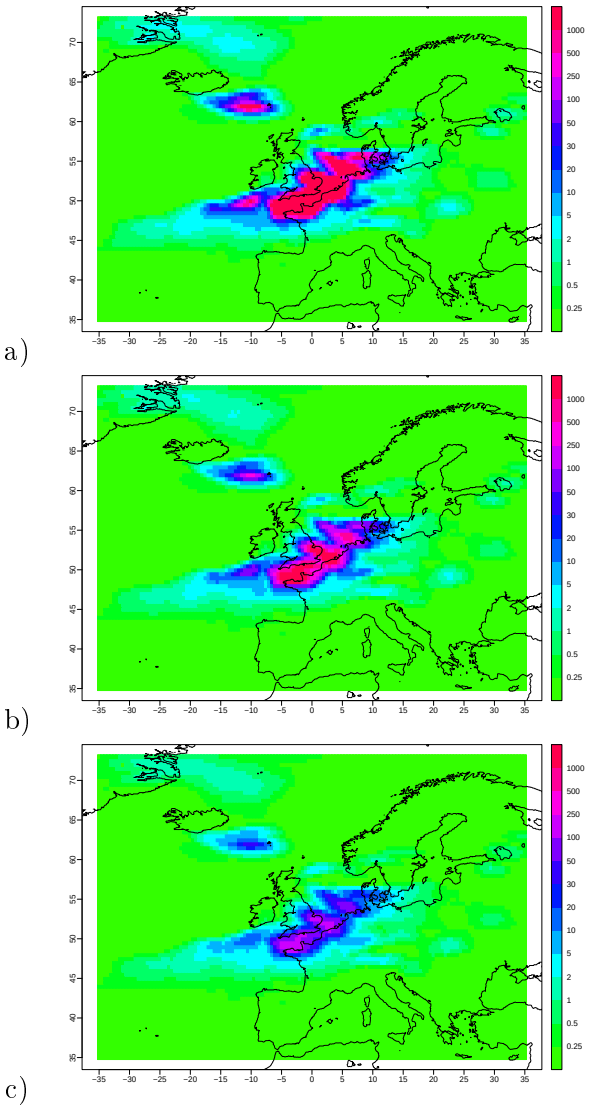

Figure 4.20: The return period (RP, years) of geostrophic wind (GW) for each grid point estimated from for the storm Daria: 19900123 1200UTC b). In a) (c) is shown the upper (lower) bound of the 95% confidence interval of the RP (years).

Figures 4.21 and 4.22 show the spatial distribution of RPs of GW associated with each storm. Some storms exhibit a more continuous spatial extent of maximum RP winds over the 72 hour period whereas others show a more 'spotty' appearance. In most cases this is due to the limitations of using the GW at 6 hourly analysis times. For example, Herta was a very fast moving mesoscale cyclone and its RP estimates are aliased due to the sampling frequency (figure 4.21c) . Another limitation of the grid point analysis that appears in these plots is the estimation of RPs of storms that are less than 72 hours apart from each other. Virtually the same spatial pattern and magnitude of RP for Vivian and Wiebke are shown in figures 4.21e and 4.21f respectively, as well as for Lothar and Martin in figures 4.22c and 4.22d. Again, this limitation is due to aliasing of the wind due to the 6 hourly resolution of the ERA-40 analysis combined with the limitation of finding the maximum RP in a 72 hour period in order to match the storms in the storm catalogue.

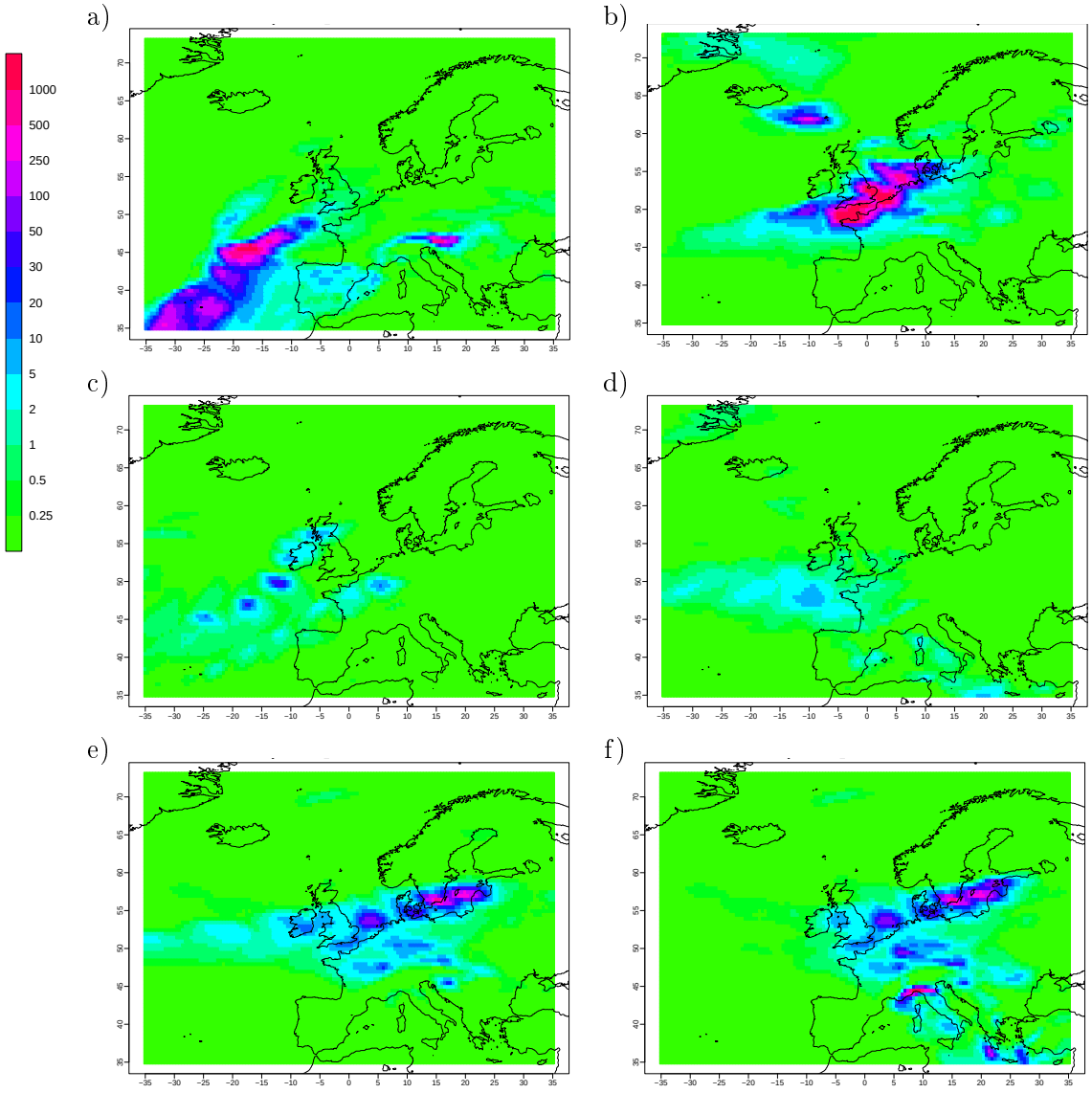

Figure 4.21: The RP (years) for each grid point for each catalogue storm in the 1990/90 October - April extended winter season estimated from *GW* and using the EVA detailed in section 3. a) unknown name: 19891215 0600UTC, b) Daria: 19900123 1200UTC , c) Herta: 19900201 0000UTC, d) Nana: 19900210 1800UTC, e) Vivian: 19900224 1200UTC, f) Wiebke: 19900226 0600UTC. The RP scale is in the top left of the plot.

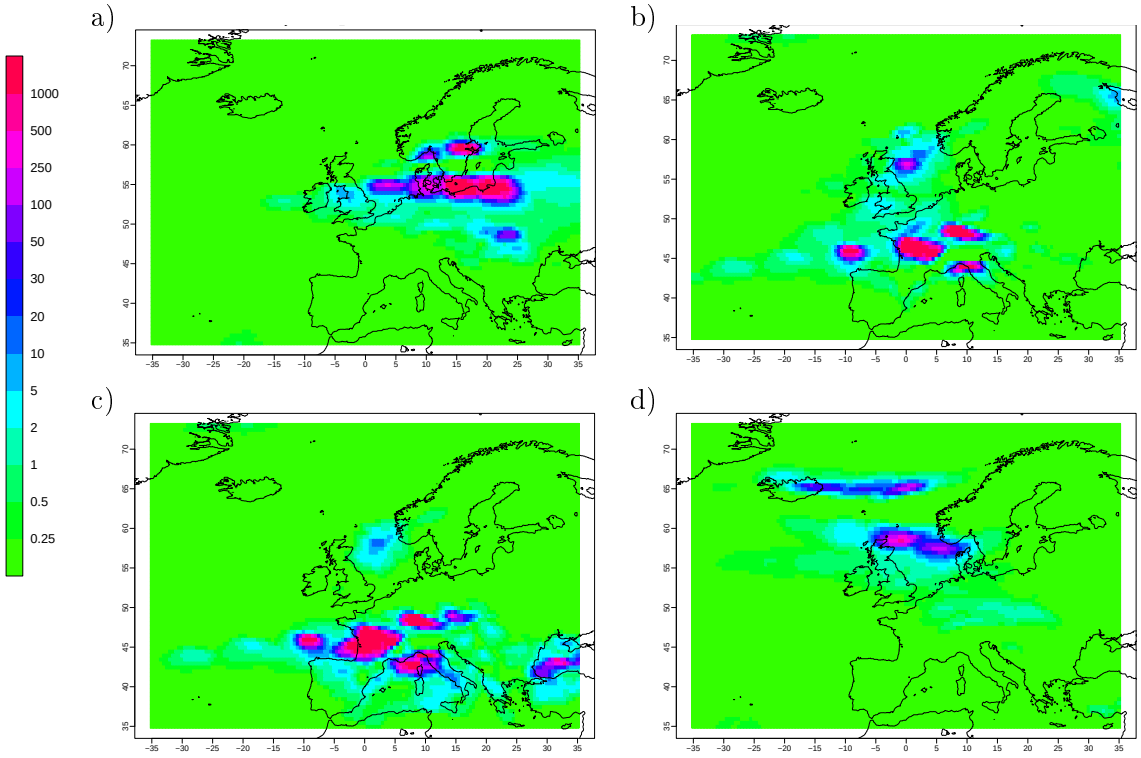

Figure 4.22: The RP (years) for each grid point for each catalogue storm in the 1999/2000 October - April extended winter season estimated from *GW* and using the EVA detailed in section 3. a) Anatol: 19991201 1200UTC, b) Lothar: 19991223 1800UTC , c) Martin: 19991225 1200UTC, d) Kerstin: 20000127 1800UTC. The RP scale is in the top left of the plot.

4.4 The evaluation of the extreme wind indices with grid point statistics

A basic evaluation of the ability of the EWI RP estimates to represent the grid point wind based RP estimates for the 96 wind storms has been performed using a Spearman rank correlation analysis. Both figures 4.23a and 4.24a show that the rank of the RPs of $Q95$ and $\bar{X}$ EWI are most highly correlated with the rank of the RPs from the grid point analysis over a region centered in the middle western part of the domain over the North Atlantic Ocean with r values in the order of 0.6. However, the rank correlation decreases radially from this point such that r over the European coast and further inland is less than about 0.25 implying that these indices can only explain 6% or less variability of the local grid point RPs. Results are better if we only consider EWI using land only grid points. Here, again we see a 'bullseye' (figures 4.23b and 4.24b) centered on western Europe roughly in the center of the land domain. Within these regions r range from 0.0 to 0.7 indicating that up to 50% of RP variations at the grid point level can be explained by the EWI.

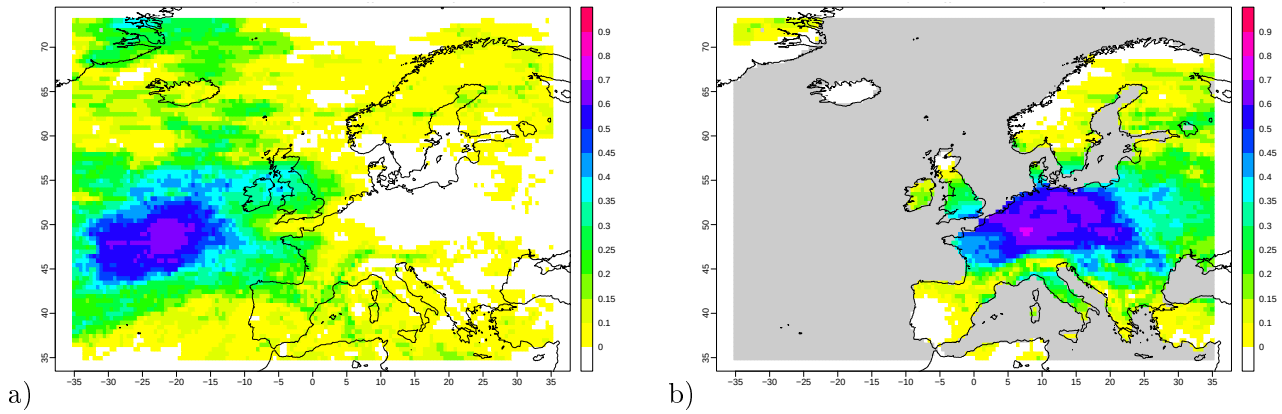

Figure 4.23: The Spearman rank correlation between the return periods of the 96 catalogue storms based on $Q95$ of GW_{72} and the return period at each grid point based on GW, a) over Δ_{all} , and b) Δ_{land}.

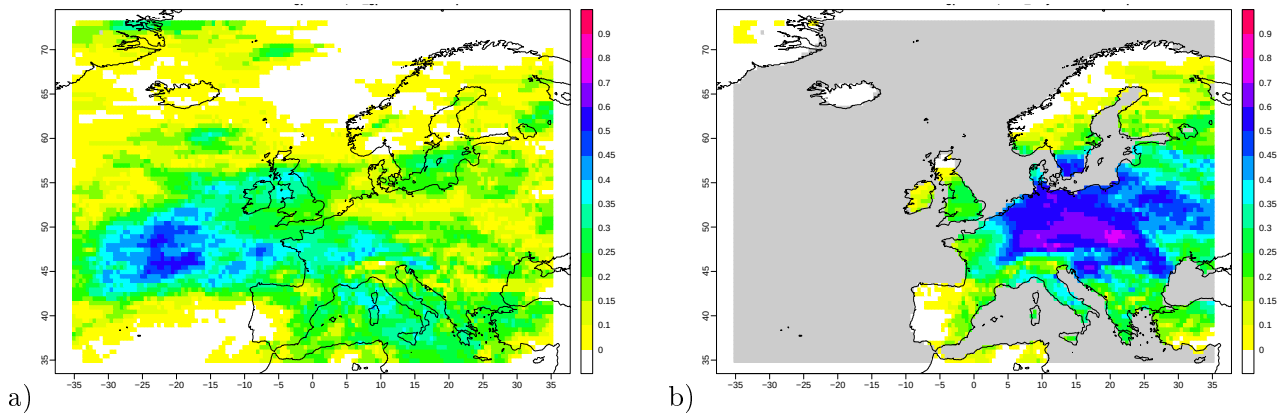

Figure 4.24: The Spearman rank correlation between the return periods of the 96 catalogue storms based on $\bar{X}$ of GW_{72} and the return period at each grid point based on GW, a) over Δ_{all} , and b) Δ_{land}.

4.5 Discussion of results

Our results show that estimating the RPs of known wind storm events is subject to many uncertainties. Firstly there is uncertainty associated with the statistical model used to describe the extreme value distribution (section 3.3), secondly there are uncertainties associated with the type of analysis performed, either using a spatial summary statistic (EWI) or individual grid point wind, and thirdly, but not least, is the effect of using different data on which to calculate these estimates.

ERA-40 derived geostrophic wind at 850hPa does not exhibit unrealistic spatial and temporal characteristics, as wind gust does over areas of complex orography, although we note that there seems to be higher magnitude winds over the Alps. We believe the flow (850hPa level) is accelerated by the smooth model orography, therefore in this area we would consider the RP estimates to be less reliable (when considering its usefulness as an indicator of surface winds) . The overall increased reliability of using geostrophic wind speed in areas of complex orography is offset to a certain extent by the aliasing effects of using 6 hourly analysis times, whereas the wind gust field is the maximum wind gust within a 6 hour period of the reanalysis. This is evident in some results from the grid point analysis.

We used the profile log-likelihood method to obtain uncertainty estimates of the RPs and showed that it gave more realistic structures to the RP uncertainty estimates than two other

commonly used approaches.

A possible shortcoming of our method of storm selection is that it is based on a statistical declustering method and therefore does not contain information about the dynamical situation which may help identification of storm events. Other methods of storm selection, for example, Lagrangian identification techniques for cyclones are also subject to many uncertainties (Raible et al., 2007). A possible alternative to the storm selection process can be found in recent literature which suggests that when using the GPD it may be possible to avoid declustering the POT series by altering the statistics used to make statistical inferences on the parameters (Fawcett and Walshaw, 2006a,b).

From the results of the EWIs it is clear that some indices performed more consistently than others (section 4.1 and table 4.1). The indices $\bar{X}$, $Sfq95$, $Sfq95q99$ have the highest inter-index and inter-dataset RP correlations, however $Q95$ has a higher spread in RP of catalogue storms. $SQ95$ should not be considered further as an suitable EWI, it consistently underestimates the RP of catalogue storms in comparison with other EWIs due to the low variability of this index. The best correlations between RPs based on the same index using different data (inter-dataset) are generally lower than the best inter-index correlations indicating that the dataset plays an important role in the calculation of the RPs. A possible explanation for these differences is the masking that is applied to WG_{72} and WG, however, we demonstrate that this has a relatively minor effect on RP differences. We suggest that the main cause of RP differences based on EWIs is a) the restrictive nature of the any spatial summary index which is not equally sensitive to all types of wind storm wind fields and b) due to fundamental differences between the WG_{72} and GW_{72} datasets. For example, the known biases in using geostrophic wind in the free atmosphere to infer severity of wind extremes at the surface (Miller, 2003). Wind gust on the other hand is a highly parameterised model forecast field and is unrealistic in areas of complex orography. A major difference between the datasets is that GW_{72} is based on the 6 hourly analysis whereas WG_{72} is a maximum over a 6 hour period. As we can see in the grid point analysis this has led to some aliasing of the extreme wind signal. Another aspect of the data which prevented a more accurate RP estimate for catalogue storms that are very close to each other in time is the 72 hour maximum wind calculation (section 2.2). This aspect of the data processing prevents the estimates of RPs from storms such as Lothar and Martin from being independent. It was noted that in many cases the catalogue storms did not match the cluster maxima of the EWI exactly. This could be due to the fact that the catalogue storm dates were chosen to simulate the time period when the storm had the highest impacts on PartnerRe assets and not necessarily when the storm had its highest intensity. In some cases a cluster maxima of the POT series indicated that a storm occurred but did not appear as a storm in the catalogue. Again, this is due to the different sampling strategy of the catalogue storms (aimed at highest impacts) and the limited number of storms able to be simulated at high resolution.

The grid point analysis produces qualitatively very similar spatial patterns of RP estimates using either GW or WG (where not masked). The grid point analysis often shows areas with much higher RPs than the RPs calculated from EWIs. This is obviously due to the effect of spatial averaging. The basic evaluation of the ability of EWIs based RP estimates to explain the RP estimates at the grid point indicate that between 0 and 50% of the grid point RP variability can be explained over continental Europe. The EWIs are sensitive to specific areas of the domain, compounding the problem of comparing RP estimates with the grid point approach. We see this as a limitation of the EWI approach, if one of the intended purposes of these indices is to try and explain local loss figures. However, we also show that the RP of catalogue storms at the grid point level is also very sensitive to the choice of wind data used. We believe that this is partly due to the aliasing problems of GW but also due to the fact that during our data processing we have interpolated the grid to 0.5° which is roughly half of the original resolution of the ERA-40 data, therefore we may be seeing sensitivity (added sampling noise) to the interpolation process at the grid point level. Better agreement might be possible using a slightly larger area average RP. When we consider that one of the fundamental questions of this study was to obtain a better

estimate of the frequency of a *wind storm,* then, given our current understanding of the problem, the EWIs offer the most valuable information. At the same time we should keep in mind that the EWI RP estimates are highly dependent on the domain chosen and as such they represent a storm which could of occurred anywhere over the domain (from a statistical point of view). Hence, *the RP of Daria* calculated using an EWI should be expressed as *the RP of a storm of Daria's magnitude to affect any part of the domain.* Whereas the grid point analysis answers the question *what is the RP of the local wind caused by Daria?*

Chapter 5

Conclusions and Recommendations for Further Research

5.1 Conclusions

MeteoSwiss have used state of the art reanalysis data combined with innovative extreme value analysis techniques to the problem of estimating the recurrence frequency of the high resolution wind storms of the PartnerRe storm catalogue. Our analysis techniques have focused only on obtaining the return period of these events, since the ERA-40 reanalysis dataset has biases associated with the magnitude of wind and wind gusts. We have shown that the generalised Pareto distribution is a robust extreme value model of the declustered peak over threshold series. The POT series was obtained using a sophisticated automatic declustering method which largely avoided the need for the specification of arbitrary parameters such is the case with more common declustering methods. We have used one of the most accurate methods in the literature to determine the uncertainty of the catalogue storm return periods.

The wind gust field of ERA-40 should be treated with extreme caution in areas where the roughness length parameter is high (> 3m), due to the boundary layer physics in the ERA-40 model. We recommend using derived geostrophic wind from the ERA-40 geopotential height field as an alternative to wind gust (although model u and v winds may also give good results) for determining the return periods of storms which affected areas where wind gust was masked.

We have tried to answer the question 'what is the return period of a particular storm event?' through the use of extreme wind indices and a grid point based approach. Neither method is completely satisfactory at answering this question. The EWIs are a spatial summary statistic and hence the return periods estimates are more representative of the return period of a *storm*, that could of occurred anywhere over the chosen domain, compared with the RP estimates derived from the grid point approach. In section 4 it was demonstrated that return period estimates for each storm, based on different indices and different base datasets in many cases varied by more than the uncertainty estimates calculated from the GPD fit. Results showed that the extreme wind indices could explain up to 50% of variations in grid point based RP estimates. The larger the domain considered the lower the effectiveness of the EWI at explaining local wind RPs. The EWI RP estimates were generally much lower than the grid point RP estimates. We conclude that it is very difficult to obtain a spatial summary statistic (EWI) which works equally well for each type of storm event in the context of trying to estimate a *storm* RP. On the other hand, the local wind grid point RPs also show dependency between datasets, due to aliasing problems and we may not be able to effectively estimate the return period of the *storm* given that no spatial dependence between grid point RPs has been modelled.

In conclusion, the results of the project demonstrate that significant progress has been made through the development of an extreme wind climatology based on a robust reanalysis dataset. We have created a climatology of wind storm RPs based on EWIs together with estimates of their local wind RP using the grid point approach. There remain considerable challenges both

from the methodological treatment of spatial extreme events and from the limitations imposed by the currently available datasets. We look forward to continuing our research to address these two issues.

5.2 Recommendations for further research

As more accurate and longer datasets of either in-situ wind data or pressure datasets become available (Diaz et al., 2002; Alexander et al., 2005; Ansell et al., 2006) this analysis should be repeated in order to minimise the uncertainty in the return period calculations. Another possible source of data which is starting to become more accessible to the climate community are ERA-40 dynamically downscaled regional climate simulations (e.g. the ENSEMBLES project). Use of this data should allow inferences about the wind gust magnitude to be made as well as a more accurate spatial assessment of the wind gust return periods (Heneka et al., 2006; Leckebusch et al., 2006, 2007; Schwierz et al., 2007). It is evident that there are some storms identified in ERA-40 which are not included in the storm catalogue that, both the EWI EVA and the grid point EVA have identified as being extreme. Further investigation of these storms either using ERA-40 or the RCM output of ENSEMBLES project could be used as a basis for adding more historical events to the storm catalogue. We also recommend further research into the spatial structure of historical wind storm events through the application of advanced spatial EVA techniques (Coles, 2001). Promising applications of Bayesian spatial extreme methods can be found in the work of Cooley et al. (2006, 2007). One should also consider using approaches that do not require the declustering of data prior to creating a POT series (Fawcett and Walshaw, 2006a,b). More research is also needed on determining the predictability of these events, either on weather or seasonal timescales (Chang et al., 2002; Wernli et al., 2002; Yan et al., 2002; Jung et al., 2005, 2006; Walser et al., 2006). Given the lack of longer and more reliable reanalysis or in-situ data, utilisation of the ever increasing amount of dynamical ensemble prediction data (van den Brink, Konnen and Opsteegh, 2004; van den Brink, Konnen, Opsteegh, van Oldenborgh and Burgers, 2004; Jung et al., 2005; Frei et al., 2006) is suggested as a means to build more realistic estimates of the frequency of wind storms.

Acknowledgements

We wish to acknowledge the reinsurance company PartnerRe who substantially sponsored this research. We wish to thank Jan Kleinn, Hervé Castella, Malcolm Haylock and Manuel Prechtl of PartnerRe for useful discussions and input to this research report. Paul Della-Marta was partially sponsored by the 6th EU framework program ENSEMBLES contract number GOCE-CT-2003-505539 and by the Swiss National Science Foundation through the National Centre for Competence in Research Climate (NCCR-Climate). The majority of the computing was performed using R statistical software.

Bibliography

Ahrens, J. H. and Dieter, U.: 1982, Computer generation of poisson deviates from modified normal distributions, *ACM Transactions on Mathematical Software* **8**, 163–179.

Albisser, P., Aller, D., Bader, S., Brnag, P., Broccard, A., Bründl, A., Dobbertin, M., Forster, B., Frutig, F., Hächler, P., Hänggli, T., Jacobi, C., Müller, E., Neu, U., Niemeyer, S., Nöthiger, C. J., Quiby, J., Rickli, C., Schilling, A., Schibiger, F. and Truog, G.: 2001, *Lothar Der Orkan 1999*, Eidg. Forchungsanstalt WSL, Bundesamt für Umwelt, Wald und Landschaft BUWAL, Birmensdorf, Bern.

Alexander, L. V., Tett, S. F. B. and Jonsson, T.: 2005, Recent observed changes in severe storms over the united kingdom and iceland, *Geophysical Research Letters* **32**(13), L13704.

Alexandersson, H. ., Schmith, T., Iden, K. and Tuomenvirta, H.: 1998, Long-term variations of the storm climate over nw europe., *Global Atmospheric and Ocean Systems* **6**, 97–120.

Alexandersson, H., Tuomenvirta, H., Schmith, T. and Iden, K.: 2000, Trends of storms in nw europe derived from an updated pressure data set, *Climate Research* **14**(1), 71–73.

Ansell, T. J., Jones, P. D., Allan, R. J., Lister, D., Parker, D. E., Brunet, M., Moberg, A., Jacobeit, J., Brohan, P., Rayner, N. A., Aguilar, E., Alexandersson, H., Barriendos, M., Brandsma, T., Cox, N. J., Della-Marta, P. M., Drebs, A., Founda, D., Gerstengarbe, F., Hickey, K., Jonsson, T., Luterbacher, J., Nordli, O., Oesterle, H., Petrakis, M., Philipp, A., Rodwell, M. J., Saladie, O., Sigro, J., Slonosky, V., Srnec, L., Swail, V., Garcia-Suarez, A. M., Tuomenvirta, H., Wang, X., Wanner, H., Werner, P., Wheeler, D. and Xoplaki, E.: 2006, Daily mean sea level pressure reconstructions for the european-north atlantic region for the period 1850-2003, *Journal Of Climate* **19**(12), 2717–2742.

Appenzeller, C., Stocker, T. F. and Anklin, M.: 1998, North atlantic oscillation dynamics recorded in greenland ice cores, *Science* **282**(5388), 446–449.

Barring, L. and von Storch, H.: 2004, Scandinavian storminess since about 1800, *Geophysical Research Letters* **31**(20), L20202.

Beersma, J. J., Rider, K. M., Komen, G. J., Kaas, E. and Kharin, V. V.: 1997, An analysis of extra-tropical storms in the north atlantic region as simulated in a control and 2xco(2) time-slice experiment with a high-resolution atmospheric model, *Tellus Series A-Dynamic Meteorology And Oceanography* **49**(3), 347–361.

Bengtsson, L., Hagemann, S. and Hodges, K. I.: 2004, Can climate trends be calculated from reanalysis data?, *Journal Of Geophysical Research-Atmospheres* **109**(D11), D11111.

Bengtsson, L., Hodges, K. I. and Roeckner, E.: 2006, Storm tracks and climate change, *Journal Of Climate* **19**(15), 3518–3543.

Bhend, J.: 2005, *North atlantic and european cyclones: Their variability and change from 1881 to 2003*, Master's thesis, Institute of Geography, University of Berne, Switzerland.

Bijl, W., Flather, R., de Ronde, J. G. and Schmith, T.: 1999, Changing storminess? an analysis of long-term sea level data sets, *Climate Research* **11**(2), 161–172.

Bouette, J. C., Chassagneux, J. F., Sibai, D., Terron, R. and Charpentier, A.: 2006, Wind in ireland: long memory or seasonal effect?, *Stochastic Environmental Research And Risk Assessment* **20**(3), 141–151.

Brabson, B. B. and Palutikof, J. P.: 2000, Tests of the generalized pareto distribution for predicting extreme wind speeds, *Journal Of Applied Meteorology* **39**(9), 1627–1640.

Caires, S. and Sterl, A.: 2005, 100-year return value estimates for ocean wind speed and significant wave height from the era-40 data, *Journal Of Climate* **18**(7), 1032–1048.

Carretero, J. C., Gomez, M., Lozano, I., de Elvira, A. R., Serrano, O., Iden, K., Reistad, M., Reichardt, H., Kharin, V., Stolley, M., von Storch, H., Gunther, H., Pfizenmayer, A., Rosethal, W., Stawarz, M., Schmith, T., Kaas, E., Li, T., Alexandersson, H., Beersma, J., Bouws, E., Komen, G., Rider, K., Flather, R., Smith, J., Bijl, W., de Ronde, J., Mietus, M., Bauer, E., Schmidt, H. and Langenberg, H.: 1998, Changing waves and storms in the northeast atlantic?, *Bulletin Of The American Meteorological Society* **79**(5), 741–760.

Chang, E. K. M., Lee, S. Y. and Swanson, K. L.: 2002, Storm track dynamics, *Journal Of Climate* **15**(16), 2163–2183.

Coles, S.: 2001, *An introduction to statistical modeling of extreme values*, Springer.

Cooley, D., Naveau, P., Jomelli, V., Rabatel, A. and Grancher, D.: 2006, A bayesian hierarchical extreme value model for lichenometry, *Environmetrics* **17**(6), 555–574.

Cooley, D., Nychka, D. and Naveau, P.: 2007, Bayesian spatial modeling of extreme precipitation return levels, *Journal of the American Statistical Association* .

Diaz, H., Folland, C., Manabe, T., Parker, D., Reynolds, R. and Woodruff, S.: 2002, Workshop on advances in the use of historical marine climate data, *CLIVAR Exchanges* **25**, 71–73.

Dukes, M. D. G. and Palutikof, J. P.: 1995, Estimation of extreme wind speeds with very long return periods, *Journal Of Applied Meteorology* **34**(9), 1950–1961.

Fawcett, L. and Walshaw, D.: 2006a, A hierarchical model for extreme wind speeds, *Journal Of The Royal Statistical Society Series C-Applied Statistics* **55**, 631–646.

Fawcett, L. and Walshaw, D.: 2006b, Markov chain models for extreme wind speeds, *Environmetrics* **17**(8), 795–809.

Ferro, C. A. T. and Segers, J.: 2003, Inference for clusters of extreme values, *Journal Of The Royal Statistical Society Series B-Statistical Methodology* **65**, 545–556.

Fisher, R. A. and Tippett, L. H. C.: 1928, Limiting forms of the frequency distribution of the largest or smallest member of a sample, *Proceedings Of The Cambridge Philosophical Society* **24**, 180–190.

Frei, C., Scholl, R., Fukutome, S., Schmidli, R. and Vidale, P. L.: 2006, Future change of precipitation extremes in europe: Intercomparison of scenarios from regional climate models, *Journal Of Geophysical Research-Atmospheres* **111**(D6), D06105.

Gillett, N. P., Allan, R. J. and Ansell, T. J.: 2005, Detection of external influence on sea level pressure with a multi-model ensemble, *Geophysical Research Letters* **32**(19), L19714.

Gillett, N. P., Zwiers, F. W., Weaver, A. J. and Stott, P. A.: 2003, Detection of human influence on sea-level pressure, *Nature* **422**(6929), 292–294.

Graybeal, D. Y.: 2006, Relationships among daily mean and maximum wind speeds, with application to data quality assurance, *International Journal Of Climatology* **26**(1), 29–43.

Held, I. M.: 1993, Large-scale dynamics and global warming, *Bulletin Of The American Meteorological Society* **74**(2), 228–241.

Heneka, P., Hofherr, T., Ruck, B. and Kottmeier, C.: 2006, Winter storm risk of residential structures-model development and application to the german state of baden-wurttemberg, *Natural Hazards And Earth System Sciences* **6**(5), 721–733.

Holton, J. R.: 2004, *An introduction to Dynamic Meteorology*, Elsevier.

Horvitz, D. G. and Thompson, D. J.: 1952, A generalization of sampling without replacement from a finite universe, *Journal of the American Statistical Association* **47**, 663–685.

Hurrel, J. W., Kushnir, Y., Ottersen, G. and Visbeck, M.: 2002, *The North Atlantic Oscillation: Climatic Significance and Environmental Impact Geophysical Monograph 134*, American Geophysical Union, Washington, DC, chapter An Overview of the North Atlantic Oscillation, pp. 1–36.

Jones, P. D., Horton, E. B., Folland, C. K., Hulme, M., Parker, D. E. and Basnett, T. A.: 1999, The use of indices to identify changes in climatic extremes, *Climatic Change* **42**(1), 131–149.

Jung, T., Gulev, S. K., Rudeva, I. and Soloviov, V.: 2006, Sensitivity of extratropical cyclone characteristics to horizontal resolution in the ecmwf model, *Quarterly Journal Of The Royal Meteorological Society* **132**(619), 1839–1857.

Jung, T., Klinker, E. and Uppala, S.: 2005, Reanalysis and reforecast of three major european storms of the twentieth century using the ecmwf forecasting system. part ii: Ensemble forecasts, *Meteorological Applications* **12**(2), 111–122.

Kaas, E., Li, T. S. and Schmith, T.: 1996, Statistical hindcast of wind climatology in the north atlantic and northwestern european region, *Climate Research* **7**, 97–110.

Kalnay, E., Kanamitsu, M., Kistler, R., Collins, W., Deaven, D., Gandin, L., Iredell, M., Saha, S., White, G., Woollen, J., Zhu, Y., Chelliah, M., Ebisuzaki, W., Higgins, W., Janowiak, J., Mo, K., Ropelewski, C., Wang, J., Leetmaa, A., Reynolds, R., Jenne, R. and Joseph, D.: 1996, The ncep/ncar 40-year reanalysis project, *Bulletin of the American Meteorological Society* **77**, 437–471.

Kasperski, M.: 2002, A new wind zone map of germany, *Journal Of Wind Engineering And Industrial Aerodynamics* **90**(11), 1271–1287.

Knippertz, P., Ulbrich, U. and Speth, P.: 2000, Changing cyclones and surface wind speeds over the north atlantic and europe in a transient ghg experiment, *Climate Research* **15**(2), 109–122.

Kristensen, L., Rathmann, O. and Hansen, S. O.: 1999, Extreme winds in denmark, *Technical report*, Riso National Laboratory.

Kunz, H., Scherrer, S. C., Liniger, M. A. and Appenzeller, C.: 2007, The evolution of era-40 surface temperatures and total ozone compared to observed swiss time series, *Meteorologische Zeitschrift* **16**, 171–181.

Lamb, H. H.: 1991, *Historic Storms of the North Sea, British Isles, and Northwest Europe*, Cambridge University Press.

Leckebusch, G. C., Koffi, B., Ulbrich, U., Pinto, J. G., Spangehl, T. and Zacharias, S.: 2006, Analysis of frequency and intensity of european winter storm events from a multi-model perspective, at synoptic and regional scales, *Climate Research* **31**(1), 59–74.

Leckebusch, G. C., Ulbrich, U., Frohlich, L. and Pinto, J. G.: 2007, Property loss potentials for european midlatitude storms in a changing climate, *Geophysical Research Letters* **34**(5), L05703.

Luterbacher, J., Xoplaki, E., Dietrich, D., Rickli, R., Jacobeit, J., Beck, C., Gyalistras, D., Schmutz, C. and Wanner, H.: 2002, Reconstruction of sea level pressure fields over the eastern north atlantic and europe back to 1500, *Climate Dynamics* **18**(7), 545–561.

Mailier, P. J., Stephenson, D. B., Ferro, C. A. T. and Hodges, K. I.: 2006, Serial clustering of extratropical cyclones, *Monthly Weather Review* **134**(8), 2224–2240.

Martins, E. S. and Stedinger, J. R.: 2000, Generalized maximum-likelihood generalized extreme-value quantile estimators for hydrologic data, *Water Resources Research* **36**(3), 737–744.

Miller, C.: 2003, A once in 50-year wind speed map for europe derived from mean sea level pressure measurements, *Journal Of Wind Engineering And Industrial Aerodynamics* **91**(12-15), 1813–1826.

Monahan, A. H.: 2004, A simple model for the skewness of global sea surface winds, *Journal Of The Atmospheric Sciences* **61**(16), 2037–2049.

Monahan, A. H.: 2006, The probability distribution of sea surface wind speeds. part 1: Theory and seawinds observations, *Journal Of Climate* **19**(4), 497–520.

Morland, J., Deuber, B., Feist, D. G., Martin, L., Nyeki, S., Kampfer, N., Matzler, C., Jeannet, P. and Vuilleumier, L.: 2006, The startwave atmospheric water database, *Atmospheric Chemistry And Physics* **6**, 2039–2056.

Palutikof, J. P., Brabson, B. B., Lister, D. H. and Adcock, S. T.: 1999, A review of methods to calculate extreme wind speeds, *Meteorological Applications* **6**(2), 119–132.

Philipp, A., Della-Marta, P. M., Jacobeit, J., Fereday, D. R., Jones, P. D., Moberg, A. and Wanner, H.: 2006, Long term variability of daily north atlantic–european pressure patterns since 1850 classified by simulated annealing clustering, *Journal of Climate* **20**(16), 4065–4095.

Pinto, J. G., Spangehl, T., Ulbrich, U. and Speth, P.: 2006, Assessment of winter cyclone activity in a transient echam4-opyc3 ghg experiment, *Meteorologische Zeitschrift* **15**(3), 279–291.

Pinto, J. G., Ulbrich, U., Leckebusch, G. C., Spangehl, T., Reyers, M. and Zacharias, S.: 2007, Changes in storm track and cyclone activity in three sres ensemble experiments with the echam5/mpi-om1 gcm, *Climate Dynamics* **29**(2-3), 195–210.

Pryor, S. C. and Barthelmie, R. J.: 2003, Long-term trends in near-surface flow over the baltic, *International Journal Of Climatology* **23**(3), 271–289.

Pryor, S. C., Schoof, J. T. and Barthelmie, R. J.: 2006, Winds of change?: Projections of near-surface winds under climate change scenarios, *Geophysical Research Letters* **33**(11), L11702.

Raible, C. C.: 2007, On the relation between extremes of midlatitude cyclones and the atmospheric circulation using era40, *Geophysical Research Letters* **34**(7), L07703.

Raible, C. C., Della-Marta, P. M., Schwierz, C., Wernli, H. and Blender, R.: 2007, Northern hemisphere midlatitude cyclones: A comparison of detection and tracking methods and different reanalyses, *Monthly Weather Review* **In Press**.

Research Triangle Institute: 2001, Sudaan user's manual, release 8.0, *Technical report*, Research Triangle Park, NC: Research Triangle Institute.

Rockel, B. and Woth, K.: 2007, Future changes in near surface wind speed extremes over europe from an ensemble of rcm simulations, *Climate Change* .

Sacré, C.: 2002, Extreme wind speed in france: the '99 storms and their consequences, *Journal Of Wind Engineering And Industrial Aerodynamics* **90**(10), 1163–1171.

Schiesser, H. H., Pfister, C. and Bader, J.: 1997, Winter storms in switzerland north of the alps 1864/1865-1993/1994, *Theoretical And Applied Climatology* **58**(1-2), 1–19.

Schinke, H.: 1993, On the occurence of deep cyclones over europe and the north atlantic in the period 1930-1991., *Beiträge zur Physik der Atmosphäre* **66**, 223–237.

Schmith, T., Kaas, E. and Li, T. S.: 1998, Northeast atlantic winter storminess 1875-1995 reanalysed, *Climate Dynamics* **14**, 529–536.

Schubiger, F., Lopez, S., Turina, A. and Romaneessen, E.: 2004, Re-analyse von extremen wetterereignissen mit dem lm ausgehend aus dem ecmwf era-40 datensatz, *DACH*.

Schwierz, C., Heck, P., Zenklusen, E., Bresch, D. N., Vidale, P., M., W. and Schär, C.: 2007, Modelling European winter wind storm losses in current and future climate, *Climatic Change* **Submitted**, 1–35.

Seierstad, I. A., Stephenson, D. B. and Kvamsto, N. G.: 2007, How useful are teleconnection patterns for explaining variability in extratropical storminess ?, *Tellus Series A-Dynamic Meteorology And Oceanography* **59**(2), 170–181.

Smits, A., Tank, A. M. G. K. and Konnen, G. P.: 2005, Trends in storminess over the netherlands, 1962-2002, *International Journal Of Climatology* **25**(10), 1331–1344.

Sterl, A.: 2004, On the (in)homogeneity of reanalysis products, *Journal Of Climate* **17**(19), 3866–3873.

Turina, A., Lopez, S., Schubiger, F., Aichinger, M. and Romaneessen, E.: 2004, High-resolution re-analysis of extreme weather events - part a: The hazard model, *Geophysical Research Abstracts, Vol. 6, 01236, 2004*.

Uppala, S. M., Kallberg, P. W., Simmons, A. J., Andrae, U., Bechtold, V. D., Fiorino, M., Gibson, J. K., Haseler, J., Hernandez, A., Kelly, G. A., Li, X., Onogi, K., Saarinen, S., Sokka, N., Allan, R. P., Andersson, E., Arpe, K., Balmaseda, M. A., Beljaars, A. C. M., Van De Berg, L., Bidlot, J., Bormann, N., Caires, S., Chevallier, F., Dethof, A., Dragosavac, M., Fisher, M., Fuentes, M., Hagemann, S., Holm, E., Hoskins, B. J., Isaksen, L., Janssen, P. A. E. M., Jenne, R., McNally, A. P., Mahfouf, J. F., Morcrette, J. J., Rayner, N. A., Saunders, R. W., Simon, P., Sterl, A., Trenberth, K. E., Untch, A., Vasiljevic, D., Viterbo, P. and Woollen, J.: 2005, The era-40 re-analysis, *Quarterly Journal Of The Royal Meteorological Society* **131**(612), 2961–3012.

van den Brink, H. W., Konnen, G. P. and Opsteegh, J. D.: 2004, Statistics of extreme synoptic-scale wind speeds in ensemble simulations of current and future climate, *Journal Of Climate* **17**(23), 4564–4574.

van den Brink, H. W., Konnen, G. P., Opsteegh, J. D., van Oldenborgh, G. J. and Burgers, G.: 2004, Improving 10(4)-year surge level estimates using data of the ecmwf seasonal prediction system, *Geophysical Research Letters* **31**(17), L17210.

Verkaik, J. W.: 2000, Evaluation of two gustiness models for exposure correction calculations, *Journal Of Applied Meteorology* **39**(9), 1613–1626.

Walser, A., Arpagaus, M., Appenzeller, C. and Leutbecher, M.: 2006, The impact of moist singular vectors and horizontal resolution on short-range limited-area ensemble forecasts for two european winter storms, *Monthly Weather Review* **134**(10), 2877–2887.

Walter, A., Keuler, K., Jacob, D., Knoche, R., Block, A., Kotlarski, S., Muller-Westermeier, G., Rechid, D. and Ahrens, W.: 2006, A high resolution reference data set of german wind velocity 1951-2001 and comparison with regional climate model results, *Meteorologische Zeitschrift* **15**(6), 585–596.

Wanner, H., Bronnimann, S., Casty, C., Gyalistras, D., Luterbacher, J., Schmutz, C., Stephenson, D. and Xoplaki, E.: 2001, North atlantic oscillation - concepts and studies, *Surveys in Geophysics* **22**, 321–382.

Weisse, R., Von Storch, H. and Feser, F.: 2005, Northeast atlantic and north sea storminess as simulated by a regional climate model during 1958-2001 and comparison with observations, *Journal Of Climate* **18**(3), 465–479.

Wernli, H., Dirren, S., Liniger, M. A. and Zillig, M.: 2002, Dynamical aspects of the life cycle of the winter storm 'lothar' (24-26 december 1999), *Quarterly Journal Of The Royal Meteorological Society* **128**(580), 405–429.

White, P.: 2003, IFS documentation cycle cy23r41, part iv: Physical processes, *Technical report*, European Center for Medium Range Forecasting.

Yan, Z., Bate, S., Chandler, R. E., Isham, V. and Wheater, H.: 2006, Changes in extreme wind speeds in nw europe simulated by generalized linear models, *Theoretical And Applied Climatology* **83**(1-4), 121–137.

Yan, Z. W., Bate, S., Chandler, R. E., Isham, V. and Wheater, H.: 2002, An analysis of daily maximum wind speed in northwestern europe using generalized linear models, *Journal Of Climate* **15**(15), 2073–2088.

Yin, J. H.: 2005, A consistent poleward shift of the storm tracks in simulations of 21st century climate, *Geophysical Research Letters* **32**(18), L18701.

Arbeitsberichte der MeteoSchweiz

215 Begert M, Seiz G, Foppa N, Schlegel T, Appenzeller C, Müller G: 2007, Die Überführung der klimatologischen Referenzstationen der Schweiz in das Swiss National Climatological Network (Swiss NBCN), 47 pp., CHF 68.-

214 Schmucki D., Weigel A., 2006, Saisonale Vorhersage in Tradition und Moderne: Vergleich der "Sommerprognose" des Zürcher Bööggs mit einem dynamischen Klimamodell, 46pp, CHF 68.-

213 Frei C: 2006, Eine Länder übergreifende Niederschlagsanalyse zum August Hochwasser 2005. Ergänzung zu Arbeitsbericht 211, 10pp, CHF 59.-

212 Z'graggen, L: 2006, Die Maximaltemperaturen im Hitzesommer 2003 und Vergleich zu früheren Extremtemperaturen, 74pp, CHF 75.-

211 MeteoSchweiz: 2006, Starkniederschlagsereignis August 2005, 63pp., CHF 72.-

210 Buss S, Jäger E and Schmutz C: 2005: Evaluation of turbulence forecasts with the aLMo, 58pp, CHF 70.–

209 Schmutz C, Schmuki D, Duding O, Rohling S: 2004, Aeronautical Climatological Information Sion LSGS, 77pp, CHF 25.–

208 Schmuki D, Schmutz C, Rohling S: 2004, Aeronautical Climatological Information Grenchen LSZG, 73pp, CHF 24.–

207 Moesch M, Zelenka A: 2004, Globalstrahlungsmessungen 1981-2000 im ANETZ, 83pp, CHF 26.–

206 Schmutz C, Schmuki D, Rohling S: 2004, Aeronautical Climatological Information St.Gallen LSZR, 78pp, CHF 25.–

205 Schmutz C, Schmuki D, Ambrosetti P, Gaia M, Rohling S: 2004, Aeronautical Climatological Information Lugano LSZA, 81pp, CHF 26.–

204 Schmuki D, Schmutz C, Rohling S: 2004, Aeronautical Climatological Information Bern LSZB, 80pp, CHF 25.–

203 Duding O, Schmuki D, Schmutz C, Rohling S: 2004, Aeronautical Climatological Information Geneva LSGG, 104pp, CHF 31.–

202 Bader S: 2004, Tropische Wirbelstürme – Hurricanes –Typhoons – Cyclones, 40pp, CHF 16.-

201 Schmutz C, Schmuki D, Rohling S: 2004, Aeronautical Climatological Information Zurich LSZH, 110pp, CHF 34.-

200 Bader S: 2004, Die extreme Sommerhitze im aussergewöhnlichen Witterungsjahr 2003, 25pp, CHF 14.-

199 Frei T, Dössegger R, Galli G, Ruffieux D: 2002, Konzept Messsysteme 2010 von MeteoSchweiz, 100pp, CHF 32.-

198 Kaufmann P: 2002, Swiss Model Simulations for Extreme Rainfall Events on the South Side of the Alps, 40pp, CHF 20.-

197 WRC Davos (Ed): 2001, IPC - IX, 25.9. - 13.10.2000, Davos, Switzerland, 100pp, CHF 32.-

196 Hächler P et al.: 1999, Der Föhnfall vom April 1993, 139pp, CHF 40.-

195 Urfer Ch, Vogt R, 1999, Die Niederschlagsverhältnisse in Basel 1964-1998, 43pp, CHF 40.-

194 Courvoisier HW: 1998, Statistik der 24-stündigen Starkniederschläge in der Schweiz 1901-1996, 20pp, CHF 11.-

193 Defila C, Vonderach G: 1998, Todesfälle und Wetterlagen in Schaffhausen, 72pp, CHF 25.-

Frühere Veröffentlichungen und Arbeitsberichte finden sich unter
www.meteoschweiz.ch » Forschung » Publikationen

Veröffentlichungen der MeteoSchweiz

77 Rossa AM: 2007, MAP-NWS – an Optional EUMETNET Programme in Support of an Optimal Research Programme, *Veröffentlichung MeteoSchweiz,* **77,** 67 pp., CHF 73.-

76 Baggenstos D: 2007, Probabilistic verification of operational monthly temperature forecasts, *Veröffentlichung MeteoSchweiz,* **76,** 52 pp.,CHF 69.-

75 Fikke S, Ronsten G, Heimo A, Kunz S, Ostrozlik M, Persson PE, Sabata J, Wareing B, Wichura B, Chum J, Laakso T, Säntti K, Makkonen L: 2007, COST 727: Atmospheric Icing on Structures Measurements and data collection on icing: State of the Art, 110pp, CHF 83.-

74 Schmutz C, Müller P, Barodte B: 2006, Potenzialabklärung für Public Private Partnership (PPP) bei MeteoSchweiz und armasuisse Immobilien, 82pp, CHF 76.-

73 Scherrer SC: 2006, Interannual climate variability in the European and Alpine region, 132pp, CHF 86.-

72 Mathis H: 2005, Impact of Realistic Greenhouse Gas Forcing on Seasonal Forecast Performance, 80pp, CHF 75.

71 Leuenberger D: 2005, High-Resolution Radar Rainfall Assimilation: Exploratory Studies with Latent Heat Nudging, 103pp, CHF 81.-

70 Müller G und Viatte P: 2005, The Swiss Contribution to the Global Atmosphere Watch Programme – Achievements of the First Decade and Future Prospects, 112pp, CHF 83.-

69 Müller WA: 2004, Analysis and Prediction of the European Winter Climate, 115pp, CHF 34.

68 Bader S: 2004, Das Schweizer Klima im Trend: Temperatur- und Niederschlagsentwicklung seit 1864, 48pp, CHF 18.-

67 Begert M, Seiz G, Schlegel T, Musa M, Baudraz G und Moesch M: 2003, Homogenisierung von Klimamessreihen der Schweiz und Bestimmung der Normwerte 1961-1990, Schlussbericht des Projektes NORM90, 170pp, CHF 40.-

66 Schär Christoph, Binder Peter, Richner Hans (Eds.): 2003, International Conference on Alpine Meteorology and MAP Meeting 2003, Extended Abstracts volumes A and B, 580pp, CHF 100.

65 Stübi R: 2002, SONDEX / OZEX campaigns of dual ozone sondes flights: Report on the data analysis, 78pp, CHF 27.-

64 Bolliger M: 2002, On the characteristics of heavy precipitation systems observed by Meteosat-6 during the MAP-SOP, 116pp, CHF 36.-

63 Favaro G, Jeannet P, Stübi R: 2002, Re-evaluation and trend analysis of the Payerne ozone sounding, 99pp, CHF 33.-

62 Bettems JM: 2001, EUCOS impact study using the limited-area non-hydrostatic NWP model in operational use at MeteoSwiss, 17pp, CHF 12.-

61 Richner H, et al.: 1999, Grundlagen aerologischer Messungen speziell mittels der Schweizer Sonde SRS 400, 140pp, CHF 42.-

60 Gisler O: 1999, Zu r Methodik einer Beschreibung der Entwicklung des linearen Trends der Lufttemperatur über der Schweiz im Zeitabschnitt von 1864 bis 1990, 125pp, CHF 36.-

59 Bettems J-M: 1999, The impact of hypothetical wind profiler networks on numerical weather prediction in the Alpine region, 65pp, CHF 25.-

58 Baudenbacher, M: 1997, Homogenisierung langer Klimareihen, dargelegt am Beispiel der Lufttemperatur, 181pp, CHF 50.-

57 Bosshard, W: 1996, Homogenisierung klimatologischer Zeitreihen, dargelegt am Beispiel der relativen Sonnenscheindauer, 136pp, CHF 38.-